Heterogeneous Cellular Network Models with Dependence

Na Deng, Wuyang Zhou, *Member, IEEE*, and Martin Haenggi, *Fellow, IEEE*

Abstract

Due to its tractability, a multi-tier model of mutually independent Poisson point processes (PPPs) for heterogeneous cellular networks (HCNs) has recently been attracting much attention. However, in reality, the locations of the BSs, within each tier and across tiers, are not fully independent. Accordingly, in this paper, we propose two HCN models with *inter-tier dependence* (Case 1) and *intra-tier dependence* (Case 2), respectively. In Case 1, the macro-BS (MBS) and the pico-BS (PBS) deployments follow a Poisson point process (PPP) and a Poisson hole process (PHP), respectively. Under this setup and conditioning on a fixed serving distance (distance between a user and its nearest serving BS), we derive bounds on the outage probabilities of both macro and pico users. We also use a fitted Poisson cluster process to approximate the PHP, which is shown to provide a good approximation of the interference and outage statistics. In Case 2, the MBSs and the PBSs follow a PPP and an independent Matern cluster process, respectively. Explicit expressions of the interference and the outage probability are derived first for fixed serving distance, second with random distance, and we derive the outage performance, the per-user capacity and the area spectral efficiency for both cases. It turns out that the proposed Case 2 model is a more appropriate and accurate model for a HCN with hotspot regions than the multi-tier independent PPP model since the latter underestimates some key performances, such as the per-user capacity and the ASE, by a factor of 1.5 to 2. Overall, the two models proposed provide good tradeoffs among the accuracy, tractability, and practicability.

Index Terms

Na Deng and Wuyang Zhou are with the Dept. of Electronic Engineering and Information Science, University of Science and Technology of China (USTC), Hefei, 230027, China (e-mail: ndeng@mail.ustc.edu.cn, wyzhou@ustc.edu.cn). Martin Haenggi is with the Dept. of Electrical Engineering, University of Notre Dame, Notre Dame 46556, USA (e-mail: mhaenggi@nd.edu).

The paper is partially under conference submission at GLOBECOM'14 [1] and WCSP'14 [2].

This work was supported by National programs for High Technology Research and Development (2012AA011402), National Natural Science Foundation of China (61172088), and by the US NSF (grants CCF 1216407 and CNS 1016742).

Stochastic geometry; heterogeneous cellular networks; Poisson point process; Poisson cluster process; outage probability; per-user capacity; area spectral efficiency.

I. Introduction

A. Motivation

To meet the crushing demands for mobile data traffic and universal seamless coverage, cellular networks are currently undergoing a major transformation from a thoroughly planned deployed to more irregular, heterogeneous deployments of macro-, pico- and femto-base stations (BSs) [3]. This increasing heterogeneity and density in cellular networks renders the traditional hexagonal and regular deployment models of limited utility but, in turn, motivates recent studies, tools and results inspired by stochastic geometry [4–6]. Most of the stochastic geometry works on cellular networks focus on the case where the BS deployment follows a homogeneous Poisson point process (PPP) for single-tier networks [7], or multiple tiers of mutually independent PPPs for heterogeneous cellular networks (HCNs) [8–10]. This means that the BSs are located independently of each other and their spatial correlation is ignored. Although the assumption of Poisson processes makes the analysis tractable, it does not seem realistic in the case of uneven population distributions and when BSs are deployed with an objective (say, capacity) that is strongly associated with user activities, which leads to dependence among the BSs including *inter-tier dependence* (i.e., the BSs belonging to different tiers exhibit repulsion) and *intra-tier dependence* (i.e., the BSs within a tier are not totally independent but planned deployments with a degree of randomness due to irregular terrains and hotspots). Therefore, models for HCNs accounting for the spatial dependence should be devised and analyzed.

B. Related Work

Although significant efforts have been made recently towards analyzing the HCNs by both academia and industry, very few works focus on the modeling of HCNs. An increasingly popular approach is to use the homogeneous PPP model from stochastic geometry to capture the irregular network topology of HCNs. The model with K independent tiers of PPP distributed BSs, i.e., the so-called HIP (homogeneous independent Poisson) model in [11], is by far the most well-understood HCN model in the literature due to its simplicity and tractability [8–10]. However, although there is randomness in the locations of small cells due to the variable capacity demands

across the coverage area, it is unrealistic to assume that the positions of the BSs are completely uncorrelated. This is because the BSs are likely to be deployed through a sophisticated network planning procedure, which results in inter-tier and intra-tier correlations among the BSs. To our best knowledge, only [12] has proposed spatial models of HCNs with dependence; they are based on the Ginibre point process (GPP) [13] whose points exhibit repulsion, accounting for the negative correlation among the BSs in different tiers and that in the same tier, respectively. However, the correlation among the BSs is not always of repulsive nature; sometimes, BSs are clustered due to increased user density. Therefore, both the inter-tier and the intra-tier dependence need to be considered when modeling the HCNs, which has been partially investigated in our previous works [1] and [2]: for the former, we propose a two-tier HCN model with inter-tier dependence, where the BSs in different tiers should be deployed at certain distance to avoid the high outage probabilities resulting from the cross-tier interference; and for the latter, we propose a two-tier HCN model with intra-tier dependence, where small cells are primarily added to increase capacity in hotspots with high user demand. Accordingly, it is unnecessary to add small cells to every macrocell; instead, they should be placed in regions where an MBS cannot offer enough capacity. The analysis in our previous works are conditioned on the distance between a user equipment (UE) and its serving BS, i.e., the serving distance, while, in this paper, we will randomize the serving distance to make the analysis more general and complete, and provide a more detailed comparison with the HIP model.

C. Contributions

The main objective of this paper is to investigate novel models that capture the spatial dependence of real HCNs, which makes them more applicable to actual network deployments than the HIP model, and to provide useful insights into the analysis and design of future wireless networks.

Specifically, we propose two two-tier HCN models with two types of BSs, i.e., MBSs and PBSs, aiming at two different cases: (1) the inter-tier dependence is considered and the small cells are primarily added to serve the edge UEs and (2) the intra-tier dependence is considered and the small cells are primarily added to increase capacity in hotspots.

In Case 1, PBSs are deployed only outside the MBS exclusion regions. This architecture, to some extent, helps reduce the inter-tier interference (because of the exclusion region), which is

one of the major challenges of HCNs. Under this setup, the MBS and the PBS deployments follow a PPP and a Poisson hole process (PHP) [4, Section 3.3], respectively. The users are uniformly distributed in the whole plane, following a PPP. Due to the inter-tier dependence, an exact calculation of the interference and outage probability seems unfeasible. Instead, two different approaches are taken to tackle this problem: one is to derive bounds on the outage probabilities of both macro users (MUs) and pico users (PUs), and the other is to approximate the PHP using fitted Poisson cluster processes (PCPs). Both approaches have their own strengths and weaknesses: the bounds derived using the first approach are tight and have closed-form expressions that are easy to calculate, while the approximations using fitted point processes provide a complete topology of the network deployments even though the resulting expressions involve multiple integrals.

In Case 2, the traffic load can have significant spatial fluctuations and clusters of PBSs are placed in hotspot regions. Under this scenario, the MBSs and the PBSs follow a PPP and an independent Matern cluster process (MCP) [4], respectively. Thereby, the intra-tier dependence is reflected by the MCP whose points exhibit clustering. For the user distribution, the user density in the hotspot regions is higher than in the rest of the network, and thus the users in the whole network form a Cox process [4]. Exact expressions of the interference and the outage probability are derived. It is observed that the model with intra-tier dependence is a more promising and practical HCN model than the HIP model for network deployments with hotspots.

In both cases, the expressions derived for the coverage probability are first conditioned on the distance between a UE and its nearest serving BS. Second, we randomize the distance between a UE and its nearest serving BS: for Case 1, we assume that an MU is uniformly distributed in the exclusion region of its nearest MBS and that the distance between a PU and its nearest PBS follows the Weibull distribution; for Case 2, both types of UEs are uniformly distributed in the disks centered at the serving BS. We find the relationship between the radius of the exclusion region and the parameter in the Weibull distribution and derive the outage probability, the per-user capacity and the area spectral efficiency (ASE) for both cases. An important observation is that both the per-user capacity and the ASE improve with smaller cells, but outage does not. By comparing the random distance case with the fixed case, we find that the trend of the outage curves are the same due to the same BS deployment. This observation indicates that the analysis of the fixed case is not only more tractable but can still provide profound insights into

the performance of HCNs.

D. Organization

The rest of the paper is organized as follows: Section II introduces the two network models with inter-tier dependence (Case 1) and intra-tier dependence (Case 2), respectively. Section III and IV present the analysis of the interference and the outage probabilities of both MUs and PUs for the two cases conditioning on the distance between a UE and its nearest serving BS, respectively. Section V explores three key performance metrics, namely the outage, the per-user capacity, and the ASE, when the distance between a UE and its serving BS is random, and Section VI offers the concluding remarks.

II. Network Model

The transmit power is μ_{m} for each MBS and μ_{p} for each PBS. The power received by a receiver located at z due to a transmitter at x is modeled as $\mu h_x \ell(x-z)$, where h_x is the power fading coefficient (square of the amplitude fading coefficient) associated with the channel between x and z, and μ is either μ_{m} or μ_{p}. We assume that the fading coefficients are i.i.d. exponential (Rayleigh fading) with $\mathbb{E}[h]=1$. $\ell(x)=\|x\|^{-\alpha}$ is the large-scale path loss model with $\alpha>2$. We focus on an MU at a distance r_{m} from the serving MBS in a random direction and a PU at a distance r_{p} from the serving PBS in a random direction. The signal-to-interference ratio (SIR) threshold is denoted as θ_{m} for MUs and θ_{p} for PUs.

A. Two-tier HCN Model with Inter-tier Dependence (Case 1)

Consider a two-tier HCN with two types of BSs, i.e., MBSs overlaid with PBSs, shown in Figure 1. The locations of the MBSs follow a homogeneous PPP $\Phi_{\mathrm{m}}=\{x_1,x_2,\ldots\}\subset\mathbb{R}^2$ of density λ_{m}, and the *potential* locations of the PBSs follow another independent homogeneous PPP $\widetilde{\Phi}_{\mathrm{p}}=\{y_1,y_2,\ldots\}\subset\mathbb{R}^2$ of density $\widetilde{\lambda}_{\mathrm{p}}$. Each MBS has an exclusion region which is a disk with radius D centered at the location of the MBS. Considering the critical issues of the current HCNs, such as interference, resource utilization and cost, PBSs are only deployed outside the exclusion regions to fill the coverage holes and thus provide better service to users, while guaranteeing that PBSs will not generate an aggregate interference resulting in the outage of macro users through designing the exclusion radius D. Under this setup, the PBSs form a point

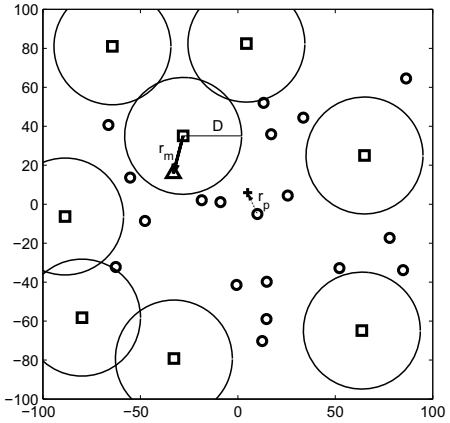

Fig. 1. The two-tier HCN model with inter-tier dependence (Case 1). The squares are the MBSs and the triangle is the typical MU at a distance $r_{\rm m}$ from its serving MBS in a random direction. The big circles are the exclusion regions with radius D. The small circles are the PBSs deployed outside the exclusion regions and the '+' is the typical PU at a distance $r_{\rm p}$ from its serving PBS in a random direction.

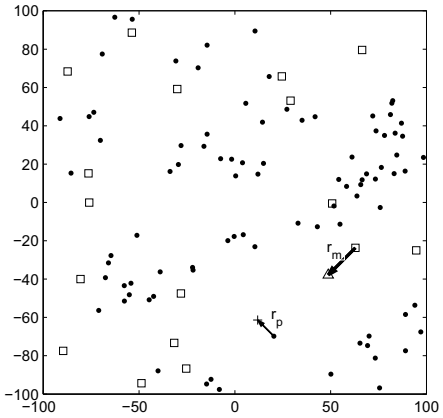

Fig. 2. The two-tier HCN model with intra-tier dependence (Case 2). The squares are the MBSs and the triangle is the typical MU at a distance $r_{\rm m}$ from its serving MBS in a random direction. The dots are the PBSs and the '+' is the typical PU at a distance $r_{\rm p}$ from its serving PBS in a random direction.

process called the *Poisson hole process*, which is a Cox process and has been used for cognitive networks [14]. We denote this process by $\Phi_{\rm p} \subset \widetilde{\Phi}_{\rm p}$ and define it as follows.

Definition 1. ***(Poisson hole process, PHP** [4, Example 3.7]) Let $\Phi_{\rm m}$ be a* PPP *of intensity $\lambda_{\rm m}$ and $\widetilde{\Phi}_{\rm p}$ be a* PPP *of intensity $\widetilde{\lambda}_{\rm p} > \lambda_{\rm m}$. For each $x \in \Phi_{\rm m}$, remove all the points in $\widetilde{\Phi}_{\rm p} \bigcap b(x, D)$, where $b(x, D)$ is a ball centered at x with radius D. Then, the remaining points of $\widetilde{\Phi}_{\rm p}$ form the Poisson hole process $\Phi_{\rm p}$. Its intensity is $\lambda_{\rm p} = \widetilde{\lambda}_{\rm p} \exp(-\lambda_{\rm m} \pi D^2)$.*

The radius D of the exclusion region is chosen as

$$D = \zeta r_{\rm m} \left(\frac{\mu_{\rm p}}{\mu_{\rm m}} \right)^{\frac{1}{\alpha}}, \tag{1}$$

where ζ is a design factor. It is intuitive why D is in this form since the radius D should be proportional to the distance between the serving MBS and its user $r_{\rm m}$ ($r_{\rm m} < D$) and the transmission power of the PBSs $\mu_{\rm p}$, and inversely proportional to the transmission power of the

MBSs $\mu_{\rm m}$. The path loss exponent should also be taken into account since it greatly affects the interference. Adding a design parameter ζ is to make the formula of D more general, which allows mimicking the concept of *Cell Range Expansion* (CRE), i.e., allowing a user to be served by a cell with weaker received power [15]. For our model, we can control the offloading from the macro to pico cells by adjusting the size of the exclusion region which determines the number of PBSs that can be retained in the HCNs. When D is set relatively large, very few potential PBSs will be retained and most users are served by the MBSs. Conversely, when D is small, the PBSs will serve more users. The value of ζ is chosen to guarantee that PBSs will not generate an aggregate interference resulting in the outage of macro users, and, conversely, the MBSs will not generate an aggregate interference resulting in the outage of PUs since the minimum distance between a MBS and a PU is $D - r_{\rm p}$.

We assume that the MBSs and the PBSs share the same spectrum, and each of them has $N_{\rm b}$ resource blocks (RBs) and serves one UE at most using one RB at a time. The users are assumed to be distributed in the whole plane according to a homogeneous PPP with density $\lambda_{\rm u}$. Under this setup, the users located within distance D of an MBS get served by MBSs within that distance, i.e., a fraction of $\kappa_{\rm m} = 1 - \exp(-\lambda_{\rm m}\pi D^2)$ of the users will be served by MBSs, and the rest are served by PBSs. We denote $N_{\rm mu}$ and $N_{\rm pu}$ as the number of UEs served by the typical MBS and the typical PBS, respectively. Due to the fact that exclusion regions may overlap, an exact calculation of the distribution of $N_{\rm mu}$ seems unfeasible. Thus, we approximate the distribution of $N_{\rm mu}$ by the Poisson distribution with mean $\kappa_{\rm m}\lambda_{\rm u}/\lambda_{\rm m}$, which is the mean of $N_{\rm mu}$, denoted as $\overline{N}_{\rm mu}$ since the average number of UEs located in the Voronoi region of a MBS is $\lambda_{\rm u}/\lambda_{\rm m}$. For the distribution of $N_{\rm pu}$ (i.e., the number of UEs located in a Voronoi region formed by a PPP with intensity $\widetilde{\Phi}_{\rm p}$), the probability generating function (PGF) is given by [16]

$$G_{N_{\rm pu}}(z) \approx \left(1 - \frac{\lambda_{\rm u}(z-1)}{\widetilde{\lambda}_{\rm p} K}\right)^{-K}. \tag{2}$$

where $K = 3.575$, and the distribution is obtained from the derivatives of $G_{N_{\rm mu}}(z)$ at zero with mean $\overline{N}_{\rm pu} = \lambda_{\rm u}/\widetilde{\lambda}_{\rm p}$. Figure 3 and 4 verify the accuracy of the approximations for the distribution of UEs when $\lambda_{\rm m} = 1.6 \times 10^{-5}$, $\lambda_{\rm p} = 8.0 \times 10^{-4}$, $\lambda_{\rm u} = 8.0 \times 10^{-4}$. We can see that for a smaller D (say, $D = 55$), the approximation is as accurate as the simulation result while for a larger D (say, $D = 95$), the distribution of $N_{\rm mu}$ can still be closely approximated.

Since $N_{\rm mu}$ and $N_{\rm pu}$ are random variables, some MBSs or PBSs will be under-utilized and

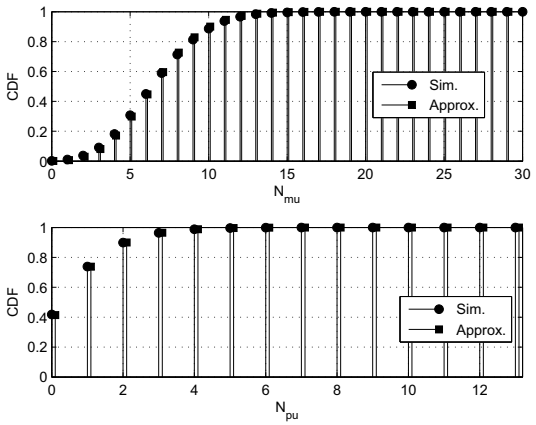

Fig. 3. The distributions of UEs for D=55.

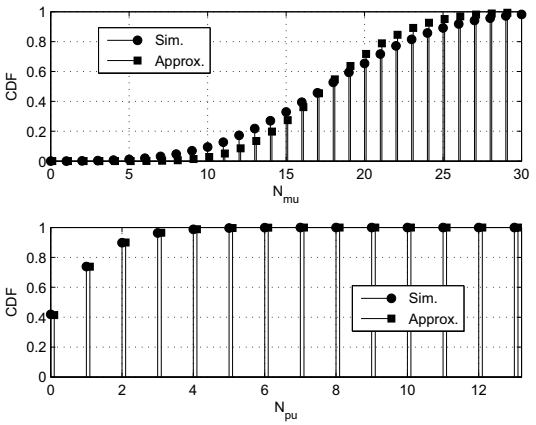

Fig. 4. The distributions of UEs for D=95.

some over-utilized. The number of the MBSs and PBSs that are using a given RB depends on the coordination and interactions among the BSs which is out of the scope of this paper. For simplicity, we assume that the RBs are uniformly and independently allocated to the UEs by each MBS and PBS, and we use the approximation $P_{\mathrm{busy,m}} \approx \min\{N_{\mathrm{b}}, \overline{N}_{\mathrm{mu}}\}/N_{\mathrm{b}}$ and $P_{\mathrm{busy,p}} \approx \min\{N_{\mathrm{b}}, \overline{N}_{\mathrm{pu}}\}/N_{\mathrm{b}}$, representing the probability that a given subchannel is used by an MBS and a PBS, respectively. In this case, the interfering MBSs (or potential PBSs, PBSs) using a certain RB constitute a point process Φ'_{m} (or $\widetilde{\Phi}'_{\mathrm{p}}$, Φ'_{p}), which can be assumed to be an independent thinning of the original process Φ_{m} (or $\widetilde{\Phi}'_{\mathrm{p}}$, Φ'_{p}) with retaining probability $P_{\mathrm{busy,m}}$ (or $P_{\mathrm{busy,p}}$) [17]. Thus, the density of Φ'_{m} (or $\widetilde{\Phi}'_{\mathrm{p}}$, Φ'_{p}) will be $\lambda'_{\mathrm{m}} = \lambda_{\mathrm{m}} P_{\mathrm{busy,m}}$ (or $\widetilde{\lambda}'_{\mathrm{p}} = \widetilde{\lambda}_{\mathrm{p}} P_{\mathrm{busy,p}}$ $\lambda'_{\mathrm{p}} = \lambda_{\mathrm{p}} P_{\mathrm{busy,p}}$), and $\Phi'_{\mathrm{p}} \subset \widetilde{\Phi}'_{\mathrm{p}}$. These two independently thinned point processes will prove useful in the subsequent analysis.

B. Two-tier HCN Model with Intra-tier Dependence (Case 2)

Consider a two-tier HCN with two types of BSs: MBSs and PBSs, shown in Figure 2, where the user density in those regions covered by PBSs (i.e., the hotspots) is higher than in the rest of the network. The locations of the MBSs follow a homogeneous PPP $\Phi_{\mathrm{m}} = \{x_1, x_2, \ldots\} \subset \mathbb{R}^2$ of density λ_{m}, and the locations of the PBSs follow an independent Matern cluster process (MCP) $\Phi_{\mathrm{p}} = \{y_1, y_2, \ldots\} \subset \mathbb{R}^2$ whose parent Poisson point process Φ_l has density λ_l. For the user distribution, the population centers of radius R are assumed to be Poisson distributed and covered using PBSs forming a MCP such that (on average) each PU can be served by its own

PBS. Denoting the average number of points per cluster as $\bar{c}$, the density of the PBSs is $\lambda_{\rm p} = \lambda_l \bar{c}$. Since points in each cluster are uniformly distributed in the circle of radius R centered at its parent point, the density of the active users, i.e., the PU density, in these population centers is $\bar{c}/(\pi R^2)$. The macro users (MUs) distributed in the rest of the network are served by their own MBSs. To facilitate the calculation, we assume that each PBS serves one PU and each MBS serves one MU in one resource block at a time, thus the densities of MUs and PUs are equal to that of the MBSs and PBSs, respectively. Under this setup, the total UEs in the network form a Cox process with density $\lambda_{\rm m}+\lambda_{\rm p}$ that are clustered in hotspots and uniformly distributed in the rest.

III. Analysis of the Two-tier HCN Model with Inter-tier Dependence

In this section, we use two different approaches to analyze the interference and outage probability of the two-tier HCN model with inter-tier dependence (Case 1) conditioning on the distance between a UE and its nearest serving BS. We first derive bounds on the outage probabilities of both MUs and PUs, and then use the fitted PCP to approximate the PHP.

There are four types of interference: the interference from the MBSs to the MUs $I_{\rm mm}$, the interference from the MBSs to the PUs $I_{\rm mp}$, the interference from the PBSs to the MUs $I_{\rm pm}$, and the interference from the PBSs to the PUs $I_{\rm pp}$. Each of them can be defined as $I(z) = \sum_{x\in\Phi\setminus\{x_0\}} \mu h_x \ell(z-x)$ to represent the interference at z resulting from the interferers positioned at the points of the process Φ (either $\Phi_{\rm m}$ or $\Phi_{\rm p}$), where x_0 is the serving BS, and μ is either $\mu_{\rm m}$ or $\mu_{\rm p}$, depending on which type of interference is considered. To calculate the interference to the MUs, we condition on having a MU at the origin, the *typical user*, i.e., there is an extra MBS, namely, the serving MBS, on the circle of radius $r_{\rm m}$ centered at o, which yields the Palm distribution for the MBSs. By Slivnyak's theorem [4], this conditional distribution is the same as the original one for the macro-tier in the region $\mathbb{R}^2 \setminus b(o, r_{\rm m})$. For the pico-tier, however, conditioning on a PBS at a certain location generally changes the distance distribution since whether a PBS is deployed is determined by the locations of the MBSs. This is the reason why only bounds or approximations through fitting the PCP can be obtained for the interference terms involving the PBSs.

A. Interference and Outage Analysis of MUs

The MUs suffer from two types of interference: I_{mm} and I_{pm}. The typical MU accesses the nearest MBS x_0, assumed at distance r_{m}. Since the fading is Rayleigh and the interfering MBSs are distributed as a PPP, the Laplace transform of I_{mm} is

$$\begin{aligned}\mathcal{L}_{I_{\mathrm{mm}}}(s) &= \mathbb{E}^{!x_0}_{\Phi'_{\mathrm{m}},h}\left(\exp\left(-s\sum_{x\in\Phi'_{\mathrm{m}}}\mu_{\mathrm{m}}h_x\ell(x)\right)\right)\\ &= \mathbb{E}^{!x_0}_{\Phi'_{\mathrm{m}}}\left(\prod_{x\in\Phi_{\mathrm{m}}}\frac{1}{1+s\mu_{\mathrm{m}}\ell(x)}\right)\\ &\overset{(a)}{=} \exp\left(-\lambda'_{\mathrm{m}}\int_{\mathbb{R}^2\setminus b(o,r_{\mathrm{m}})}\left(1-\frac{1}{1+s\mu_{\mathrm{m}}\ell(x)}\right)\mathrm{d}x\right)\\ &\overset{(b)}{=} \exp\left\{-\pi\lambda'_{\mathrm{m}}\frac{\mu_{\mathrm{m}}s\delta}{1-\delta}r_{\mathrm{m}}^{2-\alpha}F(1,1-\delta;2-\delta;-\mu_{\mathrm{m}}sr_{\mathrm{m}}^{-\alpha})\right\},\end{aligned} \tag{3}$$

where $\delta = 2/\alpha$, (a) follows from the probability generating functional (PGFL) of the PPP, which states that $\mathbb{E}[\prod_{x\in\Phi} f(x)] = \exp(-\int_{\mathbb{R}^2}(1-f(x))\Lambda(\mathrm{d}x))$ for $f:\mathbb{R}^2\to[0,1]$, and the integration regions is $\mathbb{R}^2\setminus b(o,r_{\mathrm{m}})$ since the closest interferer is at least at a distance r_{m}. $F(x,y;z;w)$ is the hypergeometric function [18], and (b) can be obtained with the help of equation (3.194.5) in [18] and a change to polar coordinates.

Since the PBSs are least at distance D from the MBSs, I_{pm} is stochastically dominated[1] by the interference $\hat{I}_{\mathrm{pm}}$ caused by the points in $\widetilde{\Phi}'_{\mathrm{p}}$ except those that are within distance D from the desired MBS. Denoting the disk centered at the location of the serving MBS with radius D as $\mathcal{H}_{\mathrm{m}}$ and letting $\mathcal{H}^{\mathcal{C}}_{\mathrm{m}} = \mathbb{R}^2\setminus\mathcal{H}_{\mathrm{m}}$, we obtain the Laplace transform of $\hat{I}_{\mathrm{pm}}$ using a modified path loss law $\widetilde{\ell}(x) = \ell(x)\mathbf{1}_{x\in\mathcal{H}^{\mathcal{C}}_{\mathrm{m}}}$ as

$$\begin{aligned}\mathcal{L}_{\hat{I}_{\mathrm{pm}}}(s) &= \mathbb{E}_{\widetilde{\Phi}'_{\mathrm{p}},h}\left(\exp\left(-s\sum_{x\in\widetilde{\Phi}'_{\mathrm{p}}}\mu_{\mathrm{p}}h_x\widetilde{\ell}(x)\right)\right)\\ &= \exp\left(-\widetilde{\lambda}'_{\mathrm{p}}\int_{\mathbb{R}^2}1-\frac{1}{1+s\mu_{\mathrm{p}}\widetilde{\ell}(x)}\mathrm{d}x\right)\\ &= \exp\left(-\widetilde{\lambda}'_{\mathrm{p}}\int_{\mathcal{H}^{\mathcal{C}}_{\mathrm{m}}}\frac{s\mu_{\mathrm{p}}\ell(x)}{1+s\mu_{\mathrm{p}}\ell(x)}\mathrm{d}x\right)\end{aligned}$$

[1]A random variable A stochastically dominates a random variable B if $\mathbb{P}(A>x)\geq\mathbb{P}(B>x)$ for all x, or, equivalently, $F_A(x)\leq F_B(x)$ for cumulative distribution functions $F_A(x)$ and $F_B(x)$.

$$= \exp\left\{-\widetilde{\lambda}'_{\mathrm{p}}\left(\frac{\pi^2\delta}{\sin(\pi\delta)}\mu_{\mathrm{p}}^{\delta}s^{\delta}-\pi D^2 A_{\mathrm{m}}(s,D)\right)\right\}, \tag{4}$$

where

$$\begin{aligned} A_{\mathrm{m}}(s,D) &= \frac{1}{\pi D^2}\int_{\mathcal{H}_{\mathrm{m}}}\left(1-\frac{1}{1+s\mu_{\mathrm{p}}\ell(|x|)}\right)\mathrm{d}x \\ &= \frac{1}{\pi D^2}\int_0^{2\pi}\int_0^{r_{\mathrm{m}}\cos\varphi+\sqrt{D^2-r_{\mathrm{m}}^2\sin^2\varphi}} \frac{r\mathrm{d}r\mathrm{d}\varphi}{1+s^{-1}\mu_{\mathrm{p}}^{-1}r^{\alpha}}. \end{aligned} \tag{5}$$

With Rayleigh fading, the transmission success probability of the MU is the Laplace transform evaluated at $s=\theta_{\mathrm{m}}\mu_{\mathrm{m}}^{-1}r_{\mathrm{m}}^{\alpha}$. Since the MBSs and the potential PBSs are distributed according to two independent PPPs, I_{mm} and $\widehat{I}_{\mathrm{pm}}$ are independent. Note that if $N_{\mathrm{b}}<N_{\mathrm{m}}$, some MUs will not be served (i.e., blocked), and their outage probability will be 1. Therefore, an upper bound for the outage probability $\epsilon_{\mathrm{m}}^{\mathrm{s}}$ of MUs who are actually served by the MBS is given by

$$\epsilon_{\mathrm{m}}^{\mathrm{s}} < 1-\mathcal{L}_{I_{\mathrm{mm}}}(\theta_{\mathrm{m}}\mu_{\mathrm{m}}^{-1}r_{\mathrm{m}}^{\alpha})\mathcal{L}_{\hat{I}_{\mathrm{pm}}}(\theta_{\mathrm{m}}\mu_{\mathrm{m}}^{-1}r_{\mathrm{m}}^{\alpha}). \tag{6}$$

When $\alpha=4$, the above bound can be simplified to

$$\epsilon_{\mathrm{m}}^{\mathrm{s}} < 1-\exp\left\{-\pi\sqrt{\theta_{\mathrm{m}}}r_{\mathrm{m}}^2\left(\lambda'_{\mathrm{m}}\arctan\sqrt{\theta_{\mathrm{m}}}+\widetilde{\lambda}'_{\mathrm{p}}\left(\frac{\pi}{2}\sqrt{\frac{\mu_{\mathrm{p}}}{\mu_{\mathrm{m}}}}-\frac{D^2}{\sqrt{\theta_{\mathrm{m}}}r_{\mathrm{m}}^2}A_{\mathrm{m}}(\theta_{\mathrm{m}}\mu_{\mathrm{m}}^{-1}r_{\mathrm{m}}^4,D)\right)\right)\right\}. \tag{7}$$

Although the point process of the PBSs is not a PPP but a Poisson hole process (see Def. 1 in Section II), independent thinning of $\widetilde{\Phi}'_{\mathrm{p}}$ outside the exclusion regions with probability $\exp(-\lambda_{\mathrm{m}}\pi D^2)$ yields a good approximation on I_{pm}, since the higher-order statistics of the point processes, which govern the interaction between the nodes, become less relevant further away from the receiver [19]. Hence,

$$\epsilon_{\mathrm{m}}^{\mathrm{s}} \approx 1-\mathcal{L}_{I_{\mathrm{mm}}}(\theta_{\mathrm{m}}\mu_{\mathrm{m}}^{-1}r_{\mathrm{m}}^{\alpha})\mathcal{L}_{\widetilde{I}_{\mathrm{pm}}}(\theta_{\mathrm{m}}\mu_{\mathrm{m}}^{-1}r_{\mathrm{m}}^{\alpha}), \tag{8}$$

where the Laplace transform of the approximation $\widetilde{I}_{\mathrm{pm}}$ is

$$\mathcal{L}_{\widetilde{I}_{\mathrm{pm}}}(s) = \exp\left\{-\lambda'_{\mathrm{p}}\left(\frac{\pi^2\delta}{\sin(\pi\delta)}\mu_{\mathrm{p}}^{\delta}s^{\delta}-\pi D^2 A_{\mathrm{m}}(s,D)\right)\right\}. \tag{9}$$

When $\alpha=4$, the approximation (8) can be simplified to

$$\epsilon_{\mathrm{m}}^{\mathrm{s}} \approx 1-\exp\left\{-\pi\sqrt{\theta_{\mathrm{m}}}r_{\mathrm{m}}^2\left(\lambda'_{\mathrm{m}}\arctan\sqrt{\theta_{\mathrm{m}}}+\lambda'_{\mathrm{p}}\left(\frac{\pi}{2}\sqrt{\frac{\mu_{\mathrm{p}}}{\mu_{\mathrm{m}}}}-\frac{D^2}{\sqrt{\theta_{\mathrm{m}}}r_{\mathrm{m}}^2}A_{\mathrm{m}}(\theta_{\mathrm{m}}\mu_{\mathrm{m}}^{-1}r_{\mathrm{m}}^4,D)\right)\right)\right\}. \tag{10}$$

Since we focus on the typical user, for the MBS considered, there is at least one user. So N_{mu} in the typical user's cell is larger by 1 compared to the N_{mu} of the typical MBS. Thus, the calculation of the outage probability of MU should be conditioned on $N_{\mathrm{mu}}\geq 1$, i.e., $P_r(N_{\mathrm{mu}}\geq$

$1) = 1 - P_r(N_{\rm mu} = 0) = 1 - e^{-\overline{N}_{\rm mu}}$ and $P_r(N_{\rm mu} = i | N_{\rm mu} \geq 1) = P_r(N_{\rm mu} = i)/P_r(N_{\rm mu} \geq 1)$. Finally, the outage probability of an arbitrary MU can be derived as

$$\epsilon_{\rm m} = \sum_{i=1}^{\infty} \left(\frac{\min\{N_{\rm b}, i\}}{i} \epsilon_{\rm m}^{\rm s} + 1 - \frac{\min\{N_{\rm b}, i\}}{i} \right) \frac{P_r(N_{\rm mu} = i)}{P_r(N_{\rm mu} \geq 1)}. \tag{11}$$

B. Interference and Outage Analysis of PUs

Similar to the interference to the MUs, the PU also experiences two types of interference: $I_{\rm mp}$ and $I_{\rm pp}$. First, we consider the interference $I_{\rm mp}$. The typical PU accesses the nearest PBS, assumed at distance $r_{\rm p}$. Denoting as $\mathcal{H}_{\rm p}$ the disk centered at the location of the serving PBS with radius D and letting $\mathcal{H}_{\rm p}^{\mathcal{C}} = \mathbb{R}^2 \setminus \mathcal{H}_{\rm p}$, we have

$$\mathcal{L}_{I_{\rm mp}}(s) = \exp\left\{ -\lambda'_{\rm m} \left(\frac{\pi^2 \delta}{\sin(\pi\delta)} \mu_{\rm m}^{\delta} s^{\delta} - \pi D^2 A_{\rm p}(s, D) \right) \right\}, \tag{12}$$

where

$$A_{\rm p}(s, D) = \frac{1}{\pi D^2} \int_0^{2\pi} \int_0^{r_{\rm p}\cos\varphi + \sqrt{D^2 - r_{\rm p}^2 \sin^2\varphi}} \frac{r {\rm d}r {\rm d}\varphi}{1 + s^{-1} \mu_{\rm m}^{-1} r^{\alpha}}. \tag{13}$$

Now let us consider the interference $I_{\rm pp}$ from the other PBSs. Letting $\hat{I}_{\rm pp}$ be the interference caused by the points in $\widetilde{\Phi}'_{\rm p}$ except those that are within the distance $r_{\rm p}$ from the typical PU, $I_{\rm pp}$ is stochastically dominated by $\hat{I}_{\rm pp}$, and its Laplace transform is

$$\begin{aligned} \mathcal{L}_{\hat{I}_{\rm pp}}(s) &= \exp\left(-\pi \widetilde{\lambda}'_{\rm p} \int_{r_{\rm p}^2}^{\infty} \frac{1}{1 + s^{-1} \mu_{\rm p}^{-1} r^{\alpha/2}} {\rm d}r \right) \\ &= \exp\left(-\pi \widetilde{\lambda}'_{\rm p} \frac{\mu_{\rm p} s \delta}{1 - \delta} r_{\rm p}^{2-\alpha} F(1, 1-\delta; 2-\delta; -\mu_{\rm p} s r_{\rm p}^{-\alpha}) \right). \end{aligned} \tag{14}$$

The success transmission probability of PUs is the Laplace transform evaluated at $s = \theta_{\rm p} \mu_{\rm p}^{-1} r_{\rm p}^{\alpha}$. Since $I_{\rm mp}$ and $\widehat{I}_{\rm pp}$ are independent, an upper bound for the outage probability $\epsilon_{\rm p}^{\rm s}$ of PUs that actually have a serving PBS can be obtained as

$$\epsilon_{\rm p}^{\rm s} < 1 - \mathcal{L}_{I_{\rm mp}}(\theta_{\rm p} \mu_{\rm p}^{-1} r_{\rm p}^{\alpha}) \mathcal{L}_{\hat{I}_{\rm pp}}(\theta_{\rm p} \mu_{\rm p}^{-1} r_{\rm p}^{\alpha}). \tag{15}$$

When $\alpha = 4$, the above bound can be simplified to

$$\epsilon_{\rm p}^{\rm s} < 1 - \exp\left\{ -\pi \sqrt{\theta_{\rm p}} r_{\rm p}^2 \left(\lambda'_{\rm p} \arctan\sqrt{\theta_{\rm p}} + \lambda'_{\rm m} \left(\frac{\pi}{2} \sqrt{\frac{\mu_{\rm m}}{\mu_{\rm p}}} - \frac{D^2}{\sqrt{\theta_{\rm p}} r_{\rm p}^2} A_{\rm p}(\theta_{\rm p} \mu_{\rm p}^{-1} r_{\rm p}^4, D) \right) \right) \right\}. \tag{16}$$

Similar to the MU, the outage probability of an arbitrary PU can be derived as

$$\epsilon_{\rm p} = \sum_{i=1}^{\infty} \left(\frac{\min\{N_{\rm b}, i\}}{i} \epsilon_{\rm p}^{\rm s} + 1 - \frac{\min\{N_{\rm b}, i\}}{i} \right) \frac{P_r(N_{\rm pu} = i)}{P_r(N_{\rm pu} > 0)}, \tag{17}$$

where $P_r(N_{\rm pu} > 0) = 1 - P_r(N_{\rm pu} = 0) = 1 - (1 + \frac{\lambda_{\rm u}}{\lambda_{\rm p} K})^{-K}$.

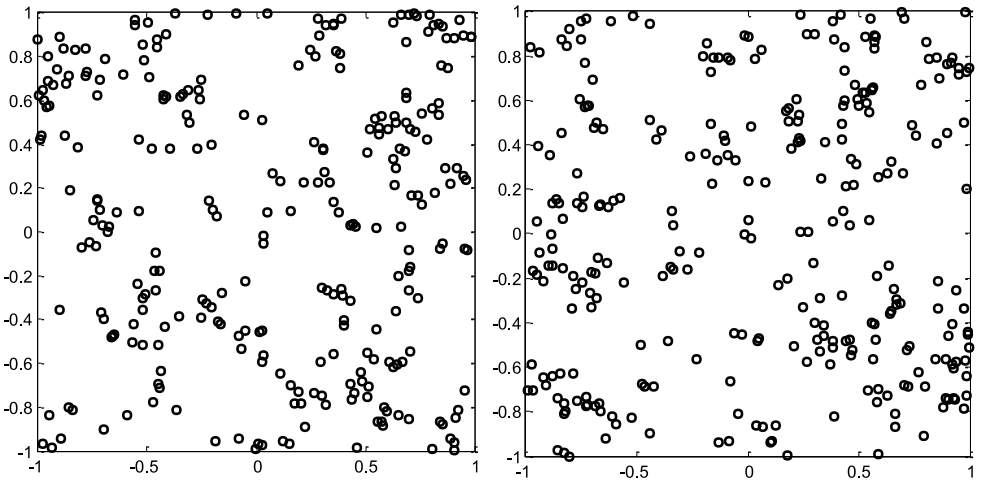

Fig. 5. Comparison of the PHP (left) and TCP (right). For the PHP, $\lambda_{\mathrm{m}} = 25$, $\widetilde{\lambda}_{\mathrm{p}} = 150$, $\mu_{\mathrm{m}} = 1$, $\mu_{\mathrm{p}} = 0.05$, $r_{\mathrm{m}} = 0.04$, $r_{\mathrm{p}} = 0.01$, $\zeta = 5$, $\alpha = 4$, $D = 0.0946$. For the TCP, $\lambda_l = 45.4734$, $\bar{c} = 1.634$, $\sigma^2 = 0.0023$.

C. Approximation by Poisson Cluster Process

The PHP behaves like a PCP to some extent, since the exclusion regions in our model force nodes to concentrate in other parts, making the whole node distribution appear clustered. The PHP is a Cox process, which is known to be overdispersed, i.e., $\mathrm{var}\,\Phi(B) \geq \mathbb{E}\Phi(B)$. Based on this, in this section, we provide another approach to approximate the outage performance of both types of users: since the PHP is not very tractable, we approximate it with a PCP by matching first- and second-order statistics. In particular, we focus on the Thomas cluster process (TCP). Figure 5 illustrates a PHP and a TCP with the same first- and second-order statistics. It is easy to observe that both processes are very different from the PPP.

1) Fitting a Poisson Cluster Process: The first-order statistic is the intensity, so

$$\lambda_{\mathrm{p}} = \widetilde{\lambda}_{\mathrm{p}} \exp(-\lambda_{\mathrm{m}} \pi D^2) = \lambda_l \bar{c}, \tag{18}$$

where λ_{p} is the intensity of the PBSs; λ_l is the density of parent points of the cluster process, and $\bar{c}$ is the average number of points in a cluster. For motion-invariant processes, the second-order statistics are fully described by the pair correlation function $g(r)$ [4]. For the TCP with variance σ^2, the g-function is [4, Section 6.4]

$$g_{\mathrm{T}}(r) = 1 + \frac{1}{4\pi\lambda_l\sigma^2} \exp\left(-\frac{r^2}{4\sigma^2}\right), \tag{19}$$

where λ_l and σ are obtained using curve-fitting and $\bar{c}$ is then determined using (18).

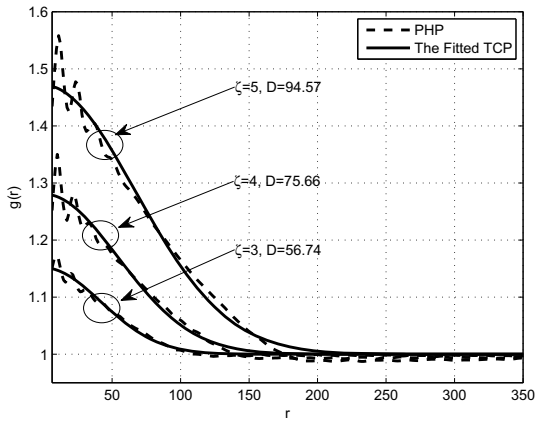

Fig. 6. Pair correlation function. $\lambda_{\rm m} = 1.6 \times 10^{-5}$, $\widetilde{\lambda}_{\rm p} = 8.0 \times 10^{-4}$, $r_{\rm m} = 40$, $r_{\rm p} = 10$, $\mu_{\rm m} = 1$, $\mu_{\rm p} = 0.05$, $\alpha = 4$.

TABLE I. The fitting results for different design factors ζ

	ζ	3	3.5	4	4.5	5	5.5
	D	56.74	66.20	75.66	85.12	94.57	104.03
Thomas	$\lambda_{\rm l}$	6.00×10^{-4}	3.10×10^{-4}	1.93×10^{-4}	1.19×10^{-4}	7.53×10^{-5}	5.44×10^{-5}
	σ^2	876.40	1220.3	1469.4	1828.4	2241.1	2509.3
	$\bar{c}$	1.130	2.062	3.098	4.672	6.755	8.512

To illustrate the fitting, we set $\lambda_{\rm m} = 1.6 \times 10^{-5}$, $\widetilde{\lambda}_{\rm p} = 8.0 \times 10^{-4}$, $r_{\rm m} = 40$, $r_{\rm p} = 10$, $\mu_{\rm m} = 1$, $\mu_{\rm p} = 0.05$, $\alpha = 4$. By using the **nlinfit** function (nonlinear least-squares fit) in Matlab, we fit the g-function of the TCP to that of the PHP for different ζ, and the fitting results are listed in Table I. It can be seen that the cluster radius R increases as D increases, which means the clustering behavior is increasingly prominent as the exclusion region becomes larger (as expected). Figure 6 shows the g-functions of the PHP and TCP obtained by simulations for $\zeta = 3, 5, 7$. The results show that the PHP can be closely approximated by the TCP.

2) Outage Analysis Using Poisson Cluster Process: Since the PHP can be closely approximated by a fitted PCP, the interference in the Poisson hole networks can be approximated by that in Poisson cluster networks. Therefore, the interference caused by $\Phi'_{\rm p}$ can be approximated by the independent thinning of the fitted PCP which keeps the density of the parent point process and independently thins every cluster with retaining probability $P_{\rm busy,p}$. Let $\bar{c}' = \bar{c}P_{\rm busy,p}$ and $\mathcal{L}_{I_{\rm pm,PCP}}(s)$ be the Laplace transform of the interference from the independent thinning of a PCP

at the typical MU located at the origin. According to [4, Cor. 4.13], we have

$$\mathcal{L}_{I_{\mathrm{pm,PCP}}}(s)=\exp\left\{-\lambda_l\int_{\mathbb{R}^2}[1-\exp(-\vec{c}'\nu(s,y))]\mathrm{d}y\right\}, \tag{20}$$

where

$$\nu(s,y)=\int_{\mathbb{R}^2}\frac{f(x)}{1+(s\mu_{\mathrm{p}}\widetilde{\ell}(x-y))^{-1}}\mathrm{d}x, \tag{21}$$

and $f(x)$ is the PDF of the node distribution around the parent point. For the TCP,

$$f(x)=\frac{1}{2\pi\sigma^2}\exp\left\{-\frac{\|x\|^2}{2\sigma^2}\right\}. \tag{22}$$

Thus the outage probability of MUs that are actually served by the MBS can be approximated as

$$\epsilon_{\mathrm{m}}^{\mathrm{s}}\approx 1-\mathcal{L}_{I_{\mathrm{mm}}}(\theta_{\mathrm{m}}\mu_{\mathrm{m}}^{-1}r_{\mathrm{m}}^{\alpha})\mathcal{L}_{I_{\mathrm{pm,PCP}}}(\theta_{\mathrm{m}}\mu_{\mathrm{m}}^{-1}r_{\mathrm{m}}^{\alpha}). \tag{23}$$

and then we can obtain the outage probability of an arbitrary MU with the same expression as Eq. (11).

Let $\mathcal{L}_{I_{\mathrm{pp,PCP}}}(s)$ be the Laplace transform of the interference from the independent thinning of a PCP at the typical PU located at the origin. Since the typical PU is served by the nearest PBS located at $(r_{\mathrm{p}},0)$, there is no PBS in the disk region centered at the origin with radius r_{p}. Thus, by denoting the modified path loss law $\widetilde{\ell}(x)=\ell(x)\mathbf{1}_{\|x\|>r_{\mathrm{p}}}$ and according to Eq. (34) in [20], we have

$$\mathcal{L}_{I_{\mathrm{pp,PCP}}}(s)=\exp\left\{-\lambda_l\int_{\mathbb{R}^2}[1-\exp(-\vec{c}'\nu(s,y))]\mathrm{d}y\right\}\int_{\mathbb{R}^2}\exp(-\vec{c}'\nu(s,y))f(y)\mathrm{d}y, \tag{24}$$

where

$$\nu(s,y)=\int_{\mathbb{R}^2}\frac{f(x)}{1+(\widetilde{\ell}(x-y)s\mu_{\mathrm{p}})^{-1}}\mathrm{d}x. \tag{25}$$

Thus, the outage probability of PUs that are actually served by the PBS can be obtained as

$$\epsilon_{\mathrm{p}}^{\mathrm{s}}\approx 1-\mathcal{L}_{I_{\mathrm{mp}}}(\theta_{\mathrm{p}}\mu_{\mathrm{p}}^{-1}r_{\mathrm{p}}^{\alpha})\mathcal{L}_{I_{\mathrm{pp,PCP}}}(\theta_{\mathrm{p}}\mu_{\mathrm{p}}^{-1}r_{\mathrm{p}}^{\alpha}). \tag{26}$$

and then we can obtain the outage probability of an arbitrary PU with the same expression as Eq. (17).

Figure 7 illustrates the outage probabilities of MUs and PUs, where $\lambda_{\mathrm{m}}=1.6\times10^{-5}$, $\widetilde{\lambda}_{\mathrm{p}}=8.0\times10^{-4}$, $\lambda_{\mathrm{u}}=0.8\times10^{-4}$, $\mu_{\mathrm{m}}=1$, $\mu_{\mathrm{p}}=0.05$, $r_{\mathrm{m}}=40$, $r_{\mathrm{p}}=10$, $\alpha=4$, $N_{\mathrm{b}}=30$, and $\zeta=3$. It can be seen that under the condition of fixed serving distance, the bounds derived for the outage probability of both types of UEs are tight, and the approximation using the fitted TCP is good.

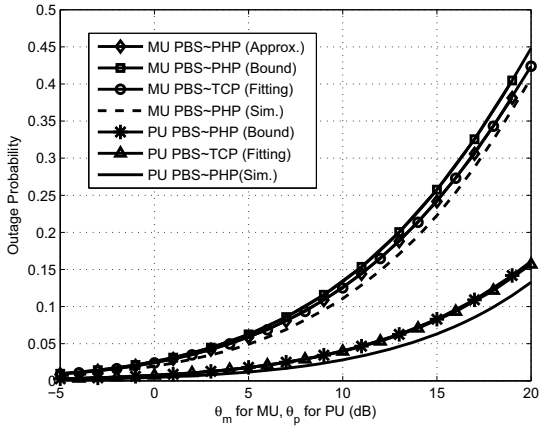

Fig. 7. Outage probabilities of MUs and PUs.

IV. Analysis of Two-tier HCN Model with Intra-tier Dependence

In this section, we first analyze the aggregate interference to both MUs and PUs, including the intra-tier interference and the inter-tier interference, and then give the outage probability for both types of UEs.

Similar to the model with inter-tier dependence, there are also four types of interference, i.e., the interference from the MBSs to the MUs I_{mm}, the interference from the MBSs to the PUs I_{mp}, the interference from the PBSs to the MUs I_{pm}, and the interference from the PBSs to the PUs I_{pp}. To calculate the interference to the MUs (or PUs), we also condition on having a typical MU (or PU) at the origin.

A. Interference and Outage Analysis of MUs

The MUs suffer from two types of interference: I_{mm} and I_{pm}. The typical MU accesses the nearest MBS x_0, assumed at distance r_{m}. Since the fading is Rayleigh and the MBSs are distributed as a PPP, the Laplace transform of I_{mm} is

$$\mathcal{L}_{I_{\mathrm{mm}}}(s)=\exp\left\{-\pi\lambda_{\mathrm{m}}\frac{\mu_{\mathrm{m}}s\delta}{1-\delta}r_{\mathrm{m}}^{2-\alpha}F(1,1-\delta;2-\delta;-\mu_{\mathrm{m}}sr_{\mathrm{m}}^{-\alpha})\right\}. \tag{27}$$

Let $\mathcal{L}_{I_{\mathrm{pm}}}(s)$ be the Laplace transform of the interference from a MCP to the typical MU located at the origin. According to [4, Cor. 4.13], we have

$$\mathcal{L}_{I_{\mathrm{pm}}}(s)=\exp\left\{-\lambda_l\int_{\mathbb{R}^2}[1-\exp(-\bar{c}\nu(s,y))]\mathrm{d}y\right\}, \tag{28}$$

where $\nu(s,y)=\int_{\mathbb{R}^2}\frac{f(x)}{1+(s\mu_{\rm p}\ell(x-y))^{-1}}{\rm d}x$, and $f(x)$ is the PDF of the node distribution around the parent point. For the MCP,

$$f(x)=\begin{cases}\frac{1}{\pi R^2}, & \|x\|<R\\ 0, & \text{otherwise.}\end{cases} \tag{29}$$

With Rayleigh fading, the transmission success probability of the MU is the Laplace transform evaluated at $s=\theta_{\rm m}\mu_{\rm m}^{-1}r_{\rm m}^{\alpha}$. Since $\Phi_{\rm m}$ and $\Phi_{\rm p}$ are independent, $I_{\rm mm}$ and $I_{\rm pm}$ are independent. Therefore, the outage probability of the MU is

$$\epsilon_{\rm m}=1-\mathcal{L}_{I_{\rm mm}}(\theta_{\rm m}\mu_{\rm m}^{-1}r_{\rm m}^{\alpha})\mathcal{L}_{I_{\rm pm}}(\theta_{\rm m}\mu_{\rm m}^{-1}r_{\rm m}^{\alpha}). \tag{30}$$

B. Interference and Outage Analysis of PUs

The PUs also experience two types of interference, i.e., $I_{\rm mp}$ and $I_{\rm pp}$. First, we consider the interference from the other PBSs $I_{\rm pp}$. Let $\mathcal{L}_{I_{\rm pp}}(s)$ be the Laplace transform of the interference from a MCP at the typical PU located at the origin. Since the typical PU is served by the nearest PBS located at $(r_{\rm p},0)$, there is no PBS in the disk centered at the origin with radius $r_{\rm p}$. Thus, using the modified path loss law $\widetilde{\ell}(x)=\ell(x)\mathbf{1}_{\|x\|>r_{\rm p}}$ and according to Eq. (34) in [20], we have

$$\mathcal{L}_{I_{\rm pp}}(s)=\exp\left\{-\lambda_l\int_{\mathbb{R}^2}[1-\exp(-\bar{c}\nu(s,y))]{\rm d}y\right\}\times\int_{\mathbb{R}^2}\exp(-\bar{c}\nu(s,y))f(y){\rm d}y, \tag{31}$$

where $\nu(s,y)=\int_{\mathbb{R}^2}\frac{f(x)}{1+(\widetilde{\ell}(x-y)s\mu_{\rm p})^{-1}}{\rm d}x$.

Now let us consider the interference from the MBSs $I_{\rm mp}$. Let $\mathcal{L}_{I_{\rm mp}}(s)$ be the Laplace transform of the interference from a PPP at the typical PU located at the origin and we have $\mathcal{L}_{I_{\rm mp}}(s)=\exp\Big(-\lambda_{\rm m}\frac{\pi^2\delta}{\sin(\pi\delta)}\mu_{\rm m}^{\delta}s^{\delta}\Big)$. The success probability of PUs is the Laplace transform evaluated at $s=\theta_{\rm p}\mu_{\rm p}^{-1}r_{\rm p}^{\alpha}$. Since $I_{\rm mp}$ and $I_{\rm pp}$ are independent, the outage probability of the PU is

$$\epsilon_{\rm p}=1-\mathcal{L}_{I_{\rm mp}}(\theta_{\rm p}\mu_{\rm p}^{-1}r_{\rm p}^{\alpha})\mathcal{L}_{I_{\rm pp}}(\theta_{\rm p}\mu_{\rm p}^{-1}r_{\rm p}^{\alpha}). \tag{32}$$

C. Comparison with the Two-tier HIP Model

Compared with the two-tier HIP model, i.e., the MBSs and PBSs follow two mutually independent homogeneous PPPs with the same densities $\lambda_{\rm m}$ and $\lambda_{\rm p}$, respectively, the only difference from our proposed model is that the PBSs are distributed as a homogeneous PPP. Under the same user distribution, in order to make this comparison relatively fair, we assume that at least one PBS is located in each hotspot region and hence model the PBSs in the two-tier HIP model as the superposition of Φ_l and another independent homogeneous PPP $\Phi_{\rm p}^{'}$ with density $\lambda_l(\bar{c}-1)$.

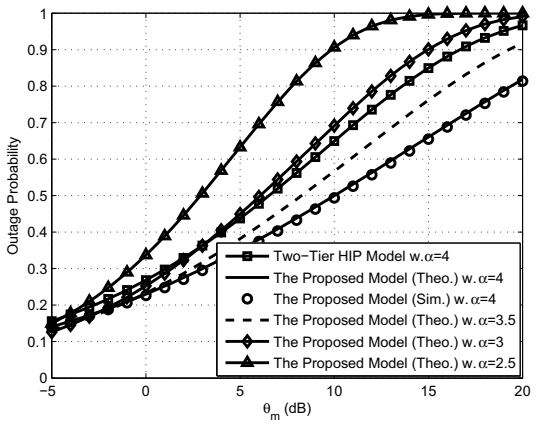

Fig. 8. The outage probability of MUs.

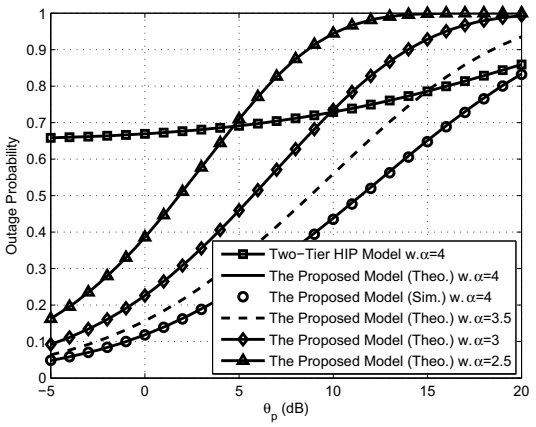

Fig. 9. The outage probability of PUs.

First, the outage probability of the MU can be easily obtained as

$$\epsilon_{\mathrm{m}} = 1 - \exp\left\{-\pi\lambda_{\mathrm{m}}\frac{\theta_{\mathrm{m}}\delta}{1-\delta}r_{\mathrm{m}}^2 F_{\mathrm{m}} - \frac{\pi^2\delta\theta_{\mathrm{m}}^{\delta}}{\sin(\pi\delta)}r_{\mathrm{m}}^2\lambda_{\mathrm{p}}\left(\frac{\mu_{\mathrm{p}}}{\mu_{\mathrm{m}}}\right)^{\delta}\right\}. \tag{33}$$

Then, for those PUs that actually have a serving PBS, the outage probability is

$$\epsilon_{\mathrm{p}}^{\mathrm{s}} = 1 - \exp\left\{-\frac{\pi^2\delta\theta_{\mathrm{p}}^{\delta}}{\sin(\pi\delta)}r_{\mathrm{p}}^2\lambda_{\mathrm{m}}\left(\frac{\mu_{\mathrm{m}}}{\mu_{\mathrm{p}}}\right)^{\delta} - \pi\lambda_{\mathrm{p}}\frac{\theta_{\mathrm{p}}\delta}{1-\delta}r_{\mathrm{p}}^2 F_{\mathrm{p}}\right\}, \tag{34}$$

and the outage probability of the PU not served (i.e. blocked) is 1. Since $\Phi_{\mathrm{p}} = \Phi_l + \Phi_{\mathrm{p}}'$, there are $N_{\mathrm{p}} = \frac{\lambda_l(\bar{c}-1)}{\lambda_l+\lambda_{\mathrm{m}}}+1$ PBSs on average in each hotspot region to serve the $\bar{c}(1+\lambda_l\pi R^2)$ PUs (i.e., the mean number of points in a disk, where the second term reflects the extra points due to the overlap). Thus, the outage probability of an arbitrary PU can be derived as

$$\epsilon_{\mathrm{p}} = \frac{N_{\mathrm{p}}}{\bar{c}(1+\lambda_l\pi R^2)}\epsilon_{\mathrm{p}}^{\mathrm{s}} + 1 - \frac{N_{\mathrm{p}}}{\bar{c}(1+\lambda_l\pi R^2)}, \tag{35}$$

Note that for the HIP model, as $\bar{c}$ increases, the number of PUs that are actually served will decrease until when $\bar{c}\to\infty$, the proportion of the served PUs reaches the maximum of $\lambda_l/((\lambda_l+\lambda_{\mathrm{m}})(1+\lambda_l\pi R^2))$.

Figure 8 and 9 illustrate the outage probabilities of MUs and PUs, respectively, for different path loss exponents α, where $\lambda_{\mathrm{m}} = \lambda_l = 8\times10^{-6}$, $\mu_{\mathrm{m}} = 1$, $\mu_{\mathrm{p}} = 0.05$, $r_{\mathrm{m}} = 40$, $r_{\mathrm{p}} = 10$, $\alpha = 4$, $\bar{c} = 20$, $R = (\pi(\lambda_{\mathrm{m}}+\lambda_l))^{-1/2}$. The simulation result matches the analytical result well, thus corroborating the accuracy of our theoretical analysis. We can observe that for both MUs and PUs, the model with larger α has better outage performance due to the fast attenuation of the interference signals. For the MU, the outage performance of the proposed model with intra-tier

dependence is superior to that of the two-tier HIP model; while for the PU, significant gains are obtained by the proposed model when $\theta_{\rm p}$ is small and the outage probability of the two-tier HIP model starts from about 0.66, which is consistent with the theoretical analysis in Section IV-C due to the parameter settings in the simulations[2]. When $\theta_{\rm p}$ is larger than about $15{\rm dB}$, the outage performance of the proposed model suffers much more serious deterioration than the independent model due to the greater interference caused by the clustering behavior among the PBSs even though the proposed model can serve more users (but, actually, most of them suffer from outage), leading to the inferior outage performance than the independent model.

V. Randomizing the Distance Between a UE and its Serving BS

The above results are all based on the condition that the distance between a UE and its nearest serving BS is fixed. In order to make the results more general and complete, we consider here the fact that the distance between a UE and its nearest serving BS is random and give the outage performance for the proposed two models with dependence. Based on the analysis of the outage, we also derive the per-user capacity and the ASE. Due to the inter-tier and intra-tier dependence, it is hard to obtain the accurate distance distribution between the UE and its serving BS. Therefore, we make some assumptions and approximations on the distance distribution in the following analysis.

A. Case 1: with Inter-Tier Dependence

In this case, the exclusion radius D is given and we assume the MUs are uniformly distributed in the circle centered at the serving MBS with the radius D, i.e., the distance $r_{\rm m}$ from the MU to its nearest serving MBS is distributed as $f_{r_{\rm m}}(t)=\frac{2t}{D^2}\mathbf{1}_{t\le D}$. As for the PU, when $D=0$, the distance $r_{\rm p}$ from the PU to the serving PBS follows the Rayleigh distribution; and when $D\to\infty$, there is no PBS and all UEs are served by the MBS. In view of the fact that Rayleigh distribution is a special case of Weibull distribution, we use the Weibull distribution to approximate the distribution of the distance between a PU and its nearest serving PBS for $D\neq 0$, i.e., we assume that $f_{r_{\rm p}}(t)=\frac{k}{\nu}\left(\frac{t}{\nu}\right)^{k-1}e^{-(t/\nu)^k}\mathbf{1}_{t\ge 0}$ [21], through adjusting the parameters k and ν for different D. Figure 10 gives the comparison between the approximation and the simulation

[2]From (35), the proportion of the PUs that are actually served is $\frac{N_{\rm p}}{\bar{c}(1+\lambda_l\pi R^2)}=\frac{\lambda_l+\lambda_{\rm m}/\bar{c}}{(\lambda_{\rm m}+2\lambda_l)}$. When $\bar{c}=20$ and $\lambda_l=\lambda_{\rm m}$, $\epsilon_p=0.35\epsilon_p^s+0.65$.

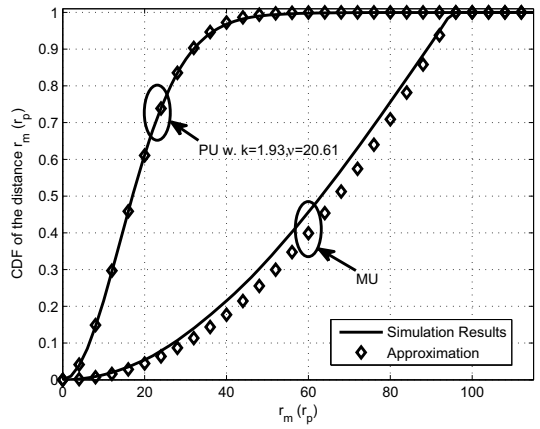

Fig. 10. Comparison between the approximation and the actual distance distribution for $D = 95$, $\lambda_{\rm m} = 1.6 \times 10^{-5}$ and $\widetilde{\lambda}_{\rm p} = 8.0 \times 10^{-4}$. The approximated distance distribution of the MU is $f_{r_{\rm m}}(t) = \frac{2t}{D^2}\mathbf{1}_{t \le D}$ with $\mathbb{E}r_{\rm m} = \frac{2}{3}D$ and that of the PU is a Weibull distribution with parameter $k = 1.93$, $\nu = 20.61$ and mean $\mathbb{E}r_{\rm p} = \nu\Gamma(1 + 1/k)$.

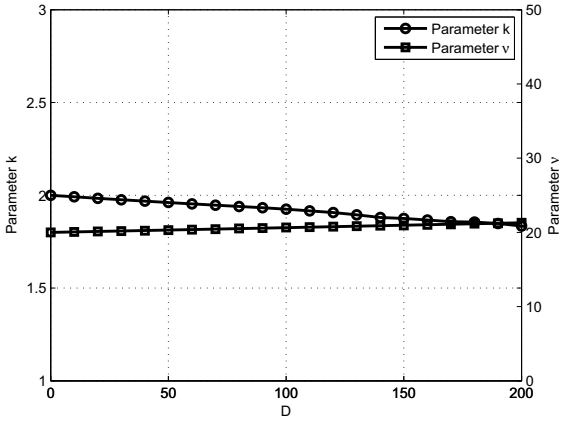

Fig. 11. The fitting parameters of Weibull distribution for the distance distribution of PU with $\lambda_{\rm m} = 1.6 \times 10^{-5}$ and $\widetilde{\lambda}_{\rm p} = 8.0 \times 10^{-4}$.

results concerning the distance distributions of both MUs and PUs, and the results show that the distance distribution of the MU and that of the PU can be closely approximated by $f_{r_{\rm m}}(t)$ and $f_{r_{\rm p}}(t)$, respectively. Figure 11 shows the relationship between the parameters of the Weibull distribution and the exclusion radius D.

1) MU: Since $f_{r_{\rm m}}(t) = \frac{2t}{D^2}\mathbf{1}_{t \le D}$, the upper bound and approximation of the outage probability can be expressed as

$$\epsilon_{\rm m}^{\rm s} < 1 - \int_0^D \mathcal{L}_{I_{\rm mm}}(\theta_{\rm m}\mu_{\rm m}^{-1}t^{\alpha})\mathcal{L}_{\hat{I}_{\rm pm}}(\theta_{\rm m}\mu_{\rm m}^{-1}t^{\alpha})\frac{2t}{D^2}{\rm d}t, \tag{36}$$

$$\epsilon_{\rm m}^{\rm s} \approx 1 - \int_0^D \mathcal{L}_{I_{\rm mm}}(\theta_{\rm m}\mu_{\rm m}^{-1}t^{\alpha})\mathcal{L}_{\tilde{I}_{\rm pm}}(\theta_{\rm m}\mu_{\rm m}^{-1}t^{\alpha})\frac{2t}{D^2}{\rm d}t. \tag{37}$$

When $\alpha = 4$, the above bound and approximation can be simplified to

$$\epsilon_{\rm m}^{\rm s} < 1 - \frac{1}{D^2}\int_0^{D^2} \exp\left(-\pi\sqrt{\theta_{\rm m}}t\left(\lambda'_{\rm m}\arctan\sqrt{\theta_{\rm m}} + \widetilde{\lambda}'_{\rm p}\left(\frac{\pi}{2}\sqrt{\frac{\mu_{\rm p}}{\mu_{\rm m}}} - \frac{D^2}{\sqrt{\theta_{\rm m}}t}A_{\rm m}(\theta_{\rm m}\mu_{\rm m}^{-1}t^2, D)\right)\right)\right){\rm d}t, \tag{38}$$

$$\epsilon_{\rm m}^{\rm s} \approx 1 - \frac{1}{D^2}\int_0^{D^2} \exp\left(-\pi\sqrt{\theta_{\rm m}}t\left(\lambda'_{\rm m}\arctan\sqrt{\theta_{\rm m}} + \lambda'_{\rm p}\left(\frac{\pi}{2}\sqrt{\frac{\mu_{\rm p}}{\mu_{\rm m}}} - \frac{D^2}{\sqrt{\theta_{\rm m}}t}A_{\rm m}(\theta_{\rm m}\mu_{\rm m}^{-1}t^2, D)\right)\right)\right){\rm d}t. \tag{39}$$

When the PHP is approximated by the PCP, the outage probability of an MU can be derived as

$$\epsilon_{\mathrm{m}}^{\mathrm{s}} \approx 1-\int_0^D \mathcal{L}_{I_{\mathrm{mm}}}(\theta_{\mathrm{m}}\mu_{\mathrm{m}}^{-1}t^{\alpha})\mathcal{L}_{I_{\mathrm{pm,PCP}}}(\theta_{\mathrm{m}}\mu_{\mathrm{m}}^{-1}t^{\alpha})\frac{2t}{D^2}\mathrm{d}t$$
$$\approx 1-\frac{1}{D^2}\int_0^{D^2} \mathcal{L}_{I_{\mathrm{mm}}}(\theta_{\mathrm{m}}\mu_{\mathrm{m}}^{-1}t^{\alpha/2})\mathcal{L}_{I_{\mathrm{pm,PCP}}}(\theta_{\mathrm{m}}\mu_{\mathrm{m}}^{-1}t^{\alpha/2})\mathrm{d}t. \quad (40)$$

Thus, the outage probability of an arbitrary MU can be obtained using Eq. (11).

2) PU: we have obtained that the Laplace transform of interference I_{mp} is

$$\mathcal{L}_{I_{\mathrm{mp}}}(s)=\exp\left\{-\lambda'_{\mathrm{m}}\left(\frac{\pi^2\delta}{\sin(\pi\delta)}\mu_{\mathrm{m}}^{\delta}s^{\delta}-\pi D^2 A_{\mathrm{p}}(s,D)\right)\right\}, \quad (41)$$

when $r_{\mathrm{p}} \leq D$

$$A_{\mathrm{p}}(s,D)=\frac{1}{\pi D^2}\int_0^{2\pi}\int_0^{r_{\mathrm{p}}\cos\varphi+\sqrt{D^2-r_{\mathrm{p}}^2\sin^2\varphi}} \frac{r\mathrm{d}r\mathrm{d}\varphi}{1+s^{-1}\mu_{\mathrm{m}}^{-1}r^{\alpha}}, \quad (42)$$

and when $r_{\mathrm{p}} > D$

$$A_{\mathrm{p}}(s,D)=\frac{2}{\pi D^2}\int_0^{\arcsin\frac{D}{r_{\mathrm{p}}}}\int_{r_{\mathrm{p}}\cos\varphi-\sqrt{D^2-r_{\mathrm{p}}^2\sin^2\varphi}}^{r_{\mathrm{p}}\cos\varphi+\sqrt{D^2-r_{\mathrm{p}}^2\sin^2\varphi}} \frac{r\mathrm{d}r\mathrm{d}\varphi}{1+s^{-1}\mu_{\mathrm{m}}^{-1}r^{\alpha}}. \quad (43)$$

Since $f_{r_{\mathrm{p}}}(t)=\frac{k}{\nu}\left(\frac{t}{\nu}\right)^{k-1}e^{-(t/\nu)^k}\mathbf{1}_{t\geq 0}$, the upper bound of the outage probability can be expressed as

$$\epsilon_{\mathrm{p}}^{\mathrm{s}} < 1-\int_0^{\infty}\mathcal{L}_{I_{\mathrm{mp}}}(\theta_{\mathrm{p}}\mu_{\mathrm{p}}^{-1}t^{\alpha})\mathcal{L}_{\hat{I}_{\mathrm{pp}}}(\theta_{\mathrm{p}}\mu_{\mathrm{p}}^{-1}t^{\alpha})\frac{k}{\nu}\left(\frac{t}{\nu}\right)^{k-1}e^{-(\frac{t}{\nu})^k}\mathrm{d}t. \quad (44)$$

When $\alpha = 4$, the above bound can be simplified as

$$\epsilon_{\mathrm{p}}^{\mathrm{s}} < 1-\int_0^{\infty}\exp\left(-\pi\sqrt{\theta_{\mathrm{p}}}\nu^2 t^{2/k}\left(\widetilde{\lambda}'_{\mathrm{p}}\arctan\sqrt{\theta_{\mathrm{p}}}+\lambda'_{\mathrm{m}}\left(\frac{\pi}{2}\sqrt{\frac{\mu_{\mathrm{m}}}{\mu_{\mathrm{p}}}}-\frac{D^2 A_{\mathrm{p}}(\theta_{\mathrm{p}}\mu_{\mathrm{p}}^{-1}\nu^4 t^{4/k},D)}{\sqrt{\theta_{\mathrm{p}}}\nu^2 t^{2/k}}\right)\right)-t\right)\mathrm{d}t. \quad (45)$$

When the PHP is approximated by a PCP, the outage probability can be obtained as

$$\epsilon_{\mathrm{p}}^{\mathrm{s}} \approx 1-\int_0^{\infty}\mathcal{L}_{I_{\mathrm{mp}}}(\theta_{\mathrm{p}}\mu_{\mathrm{p}}^{-1}\nu^{\alpha}t^{\alpha/k})\mathcal{L}_{I_{\mathrm{pp,PCP}}}(\theta_{\mathrm{p}}\mu_{\mathrm{p}}^{-1}\nu^{\alpha}t^{\alpha/k})e^{-t}\mathrm{d}t. \quad (46)$$

Thus, the outage probability of an arbitrary PU can be obtained using Eq. (17).

3) Per-user Capacity and ASE: According to our network model, we know that N_{p} PBSs serve N_{pu} PUs and each MBS serves N_{mu} MUs on average in a macrocell. Letting $\kappa_{\mathrm{p}} = 1-\kappa_{\mathrm{m}}$ denote the fraction of the PUs of the total UEs, where $\kappa_{\mathrm{m}} = 1-\exp(-\lambda_{\mathrm{m}}\pi D^2)$, the per-user capacity for a fixed-rate transmission based on the SIR threshold of the MU and PU, respectively, are

$$c_{\mathrm{m}} = \frac{1}{N_{\mathrm{b}}}(1-\epsilon_{\mathrm{m}})\log_2(1+\theta_{\mathrm{m}}), \quad (47)$$

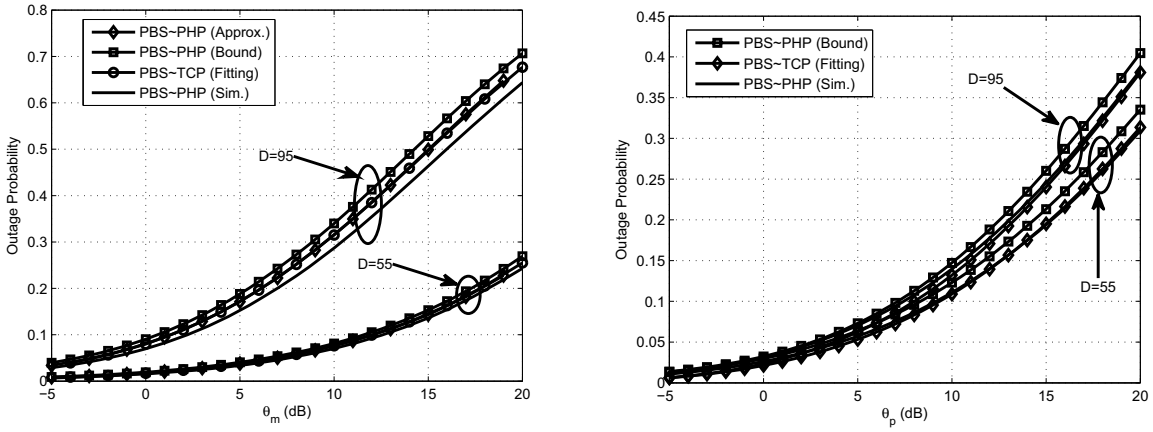

(a) Outage probability of MU.

(b) Outage probability of PU.

Fig. 12. Case 1: Model with inter-tier dependence for random serving distance.

$$c_{\mathrm{p}} = \frac{1}{N_{\mathrm{b}}}(1-\epsilon_{\mathrm{p}})\log_2(1+\theta_{\mathrm{p}}). \tag{48}$$

Thus, the overall per-user capacity c_{u} is given by

$$\begin{aligned} c_{\mathrm{u}} =& \kappa_{\mathrm{m}} c_{\mathrm{m}} + \kappa_{\mathrm{p}} c_{\mathrm{p}} \\ =& \frac{\kappa_{\mathrm{m}}}{N_{\mathrm{b}}}(1-\epsilon_{\mathrm{m}})\log_2(1+\theta_{\mathrm{m}}) + \frac{\kappa_{\mathrm{p}}}{N_{\mathrm{b}}}(1-\epsilon_{\mathrm{p}})\log_2(1+\theta_{\mathrm{p}}). \end{aligned} \tag{49}$$

Finally, the ASE of the model with inter-tier dependence can be defined as [22]

$$\mathrm{ASE} = \lambda_{\mathrm{m}}\frac{\overline{N}_{\mathrm{mu}}}{N_{\mathrm{b}}}(1-\epsilon_{\mathrm{m}})\log_2(1+\theta_{\mathrm{m}}) + \lambda_{\mathrm{p}}\frac{\overline{N}_{\mathrm{pu}}}{N_{\mathrm{b}}}(1-\epsilon_{\mathrm{p}})\log_2(1+\theta_{\mathrm{p}}). \tag{50}$$

In the following, we give some numerical results of the outage probability for MU and PU, the per-user capacity, and the area spectral efficiency for Case 1 with random serving distance, where the default parameters are set as $\lambda_{\mathrm{m}} = 1.6 \times 10^{-5}$, $\widetilde{\lambda}_{\mathrm{p}} = 8.0 \times 10^{-4}$, $\lambda_{\mathrm{u}} = 8.0 \times 10^{-4}$, $\mu_{\mathrm{m}} = 1$, $\mu_{\mathrm{p}} = 0.05$, $\alpha = 4$, $N_{\mathrm{b}} = 50$, $D = 55$.

Figure 12 illustrates the outage probabilities of MUs and PUs for the inter-tier dependence model with random distance between the UE and its nearest serving BS and different exclusion radii D. We can observe that for the more general case (i.e., random serving distance), the bounds derived for the outage probability of both types of UEs are quite tight and the approximation using the fitted TCP matches the simulation result very well, especially for smaller D (say, $D = 55$), which verifies that the PCP can model the PHP accurately and a good estimate of the

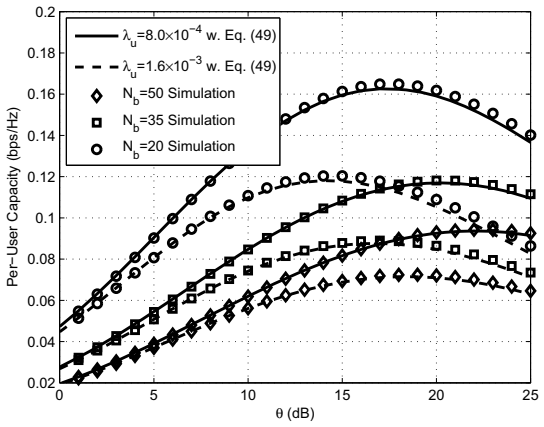

Fig. 13. Case 1: per-user capacity versus user threshold, where $\theta_{\mathrm{m}} = \theta_{\mathrm{p}} = \theta$.

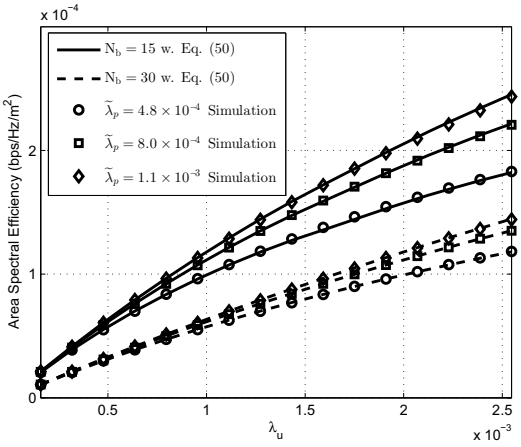

Fig. 14. Case 1: area spectral efficiency versus user density.

interference can be obtained. Comparing Figure 12(a) with Figure 12(b), we find that the radius of the exclusion region affects the performance of the MUs more strongly than that of the PUs. This is because, the exclusion radius has a direct effect on the number of UEs accessing the MBS while the quality of service (QoS) of the UEs, i.e., the outage performance, is limited by the available resources.

Figure 13 shows the relationship between the per-user capacity and the user threshold ($\theta_{\mathrm{m}} = \theta_{\mathrm{p}} = \theta$) for different number of RBs N_{b} and user densities λ_{u}. We observe that models with a smaller λ_{u} have higher per-user capacity due to the sufficient available resources relative to the user density and smaller interference resulting from the smaller probability that a given subchannel is occupied. In addition, as N_{b} increases, the per-user capacity decreases since the available spectrum is fixed, then the more N_{b} is, the less spectrum resource is allocated to each UE.

Figure 14 depicts how the ASE changes with the user density λ_{u} for different $\widetilde{\lambda}_{\mathrm{p}}$ and N_{b} when $\theta_{\mathrm{m}} = \theta_{\mathrm{p}} = 5\mathrm{dB}$. It is seen that the ASE increases with the density of potential PBSs and the user density but decreases with N_{b}, which indicates that a good ASE comes from the proper matching between the network deployment as well as resource allocation and the user density (i.e., the traffic demand), and small cells improves the ASE. Although increasing N_{b} can reduce the probability that a given subchannel is occupied and further the interference from both MBSs and PBSs, the ASE contributed by the reduction of the interference can not compensate

with the loss caused by the reduction of the bandwidth obtained by each UE. By comparing Figure 13 with Figure 14, we find that the ASE improves with the increasing of the user density, while the per-user capacity does not. Since picocell is not capacity-limited, i.e., $\lambda_{\rm u}/\lambda_{\rm p} \ll N_{\rm b}$, the density of the interfering sources $\lambda_{\rm p}\min(\lambda_{\rm u}/\lambda_{\rm p}, N_{\rm b})/N_{\rm b}$ only depends on $\lambda_{\rm u}$ and $N_{\rm b}$. So as $\lambda_{\rm u}$ increases, the density of the interferers increases, causing more interference to each UE and reducing the per-user capacity, but, conversely, the number of UEs served is increasing, which leads to the increase of the ASE finally.

B. Case 2: with Intra-Tier Dependence

From the description of the proposed model with intra-tier dependence, the average coverage area of each MBS or each cluster of PBSs is $1/(\lambda_l + \lambda_{\rm m})$, and since there are $\bar{c}$ PBSs in one cluster on average, the average coverage area of each PBS is $\frac{1}{\bar{c}(\lambda_l+\lambda_{\rm m})}$. The coverage regions of the MBS and PBS are approximated by circular regions and the corresponding radii are $D_{\rm m} = 1/\sqrt{\pi(\lambda_l+\lambda_{\rm m})}$ and $D_{\rm p} = D_{\rm m}/\sqrt{\bar{c}}$, respectively. We assume that the MU is uniformly distributed in the circle centered at the serving MBS with the radius $D_{\rm m}$ and the PU is uniformly distributed in the circle centered at the serving PBS with the radius $D_{\rm p}$. Though simple and inaccurate to some extent, the assumptions can reflect the stochastic behavior of the distance between a UE and its serving BS and the UE aggregation behavior.

1) MU: Since the MU is uniformly distributed in the circle centered at the serving MBS with the radius $D_{\rm m}$, the outage probability can be obtained as

$$\begin{aligned}\epsilon_{\rm m} &= 1-\int_0^{D_{\rm m}} \mathcal{L}_{I_{\rm mm}}(\theta_{\rm m}\mu_{\rm m}^{-1}t^{\alpha})\mathcal{L}_{I_{\rm pm}}(\theta_{\rm m}\mu_{\rm m}^{-1}t^{\alpha})\frac{2t}{D_{\rm m}^2}{\rm d}t \\ &= 1-\frac{1}{D_{\rm m}^2}\int_0^{D_{\rm m}^2} \mathcal{L}_{I_{\rm mm}}(\theta_{\rm m}\mu_{\rm m}^{-1}t^{\alpha/2})\mathcal{L}_{I_{\rm pm}}(\theta_{\rm m}\mu_{\rm m}^{-1}t^{\alpha/2}){\rm d}t. \end{aligned} \tag{51}$$

2) PU: The outage probability of a PU is

$$\epsilon_{\rm p}=1-\frac{1}{D_{\rm p}^2}\int_0^{D_{\rm p}^2} \mathcal{L}_{I_{\rm mp}}(\theta_{\rm p}\mu_{\rm p}^{-1}t^{\alpha/2})\mathcal{L}_{I_{\rm pp}}(\theta_{\rm p}\mu_{\rm p}^{-1}t^{\alpha/2}){\rm d}t. \tag{52}$$

3) Per-user Capacity and ASE: According to the descriptions of the model, since the densities of MUs and PUs are equal to that of MBSs and PBSs, respectively, and the PUs are concentrated in the densely populated regions, the MUs take the proportion $\kappa_{\rm m} = \frac{\lambda_{\rm m}}{\lambda_{\rm m}+\lambda_{\rm p}}$ of the total UEs and the proportion of PUs is $\kappa_{\rm p} = 1-\kappa_{\rm m}$. Then, we obtain the per-user capacity of the MU and PU

for a fixed-rate transmission based on the SIR threshold, respectively, as follows,

$$c_{\mathrm{m}} = (1-\epsilon_{\mathrm{m}})\log_2(1+\theta_{\mathrm{m}}), \tag{53}$$

$$c_{\mathrm{p}} = (1-\epsilon_{\mathrm{p}})\log_2(1+\theta_{\mathrm{p}}). \tag{54}$$

Thus, the overall per-user capacity c_{u} is given by

$$\begin{aligned} c_{\mathrm{u}} =& \kappa_{\mathrm{m}} c_{\mathrm{m}} + \kappa_{\mathrm{p}} c_{\mathrm{p}} \\ =& \frac{\lambda_{\mathrm{m}}(1-\epsilon_{\mathrm{m}})\log_2(1+\theta_{\mathrm{m}}) + \lambda_{\mathrm{p}}(1-\epsilon_{\mathrm{p}})\log_2(1+\theta_{\mathrm{p}})}{\lambda_{\mathrm{m}}+\lambda_{\mathrm{p}}}. \end{aligned} \tag{55}$$

Finally, the area spectral efficiency (ASE) of the proposed model with intra-tier dependence can be defined as

$$\mathrm{ASE} = \lambda_{\mathrm{m}}(1-\epsilon_{\mathrm{m}})\log_2(1+\theta_{\mathrm{m}}) + \lambda_{\mathrm{p}}(1-\epsilon_{\mathrm{p}})\log_2(1+\theta_{\mathrm{p}}). \tag{56}$$

4) Comparison with the Two-tier HIP Model: First, the outage probability of the MU can be easily obtained as

$$\begin{aligned} \epsilon_{\mathrm{m}} =& 1 - \int_0^{D_{\mathrm{m}}} \exp\left(-\pi\lambda_{\mathrm{m}} \int_{t^2}^{\infty} \frac{1}{1+\theta_{\mathrm{m}}^{-1} t^{-\alpha} r^{\alpha/2}} \mathrm{d}r - \frac{\pi^2\delta}{\sin(\pi\delta)} \theta_{\mathrm{m}}^{\delta} t^2 \lambda_{\mathrm{p}} (\mu_{\mathrm{p}}/\mu_{\mathrm{m}})^{\delta}\right) \frac{2t}{D_{\mathrm{m}}^2} \mathrm{d}t \\ =& 1 - \frac{1}{D_{\mathrm{m}}^2} \frac{1 - e^{-\pi\lambda_{\mathrm{m}} \frac{\theta_{\mathrm{m}}\delta}{1-\delta} D_{\mathrm{m}}^2 F_{\mathrm{m}} - \frac{\pi^2\delta}{\sin(\pi\delta)} \theta_{\mathrm{m}}^{\delta} \lambda_{\mathrm{p}} (\mu_{\mathrm{p}}/\mu_{\mathrm{m}})^{\delta} D_{\mathrm{m}}^2}}{\pi\lambda_{\mathrm{m}} \frac{\theta_{\mathrm{m}}\delta}{1-\delta} F_{\mathrm{m}} + \frac{\pi^2\delta}{\sin(\pi\delta)} \theta_{\mathrm{m}}^{\delta} \lambda_{\mathrm{p}} (\mu_{\mathrm{p}}/\mu_{\mathrm{m}})^{\delta}}, \end{aligned} \tag{57}$$

and the outage probability of the PU is

$$\begin{aligned} \epsilon_{\mathrm{p}}^{\mathrm{s}} =& 1 - \int_0^{D_{\mathrm{p}}} \exp\left(-\frac{\pi^2\delta}{\sin(\pi\delta)} \theta_{\mathrm{p}}^{\delta} t^2 \lambda_{\mathrm{m}} (\mu_{\mathrm{m}}/\mu_{\mathrm{p}})^{\delta} - \pi\lambda_{\mathrm{p}} \int_{t^2}^{\infty} \frac{1}{1+\theta_{\mathrm{p}}^{-1} t^{-\alpha} r^{\alpha/2}} \mathrm{d}r\right) \frac{2t}{D_{\mathrm{p}}^2} \mathrm{d}t \\ =& 1 - \frac{1}{D_{\mathrm{p}}^2} \frac{1 - e^{-\pi\lambda_{\mathrm{p}} \frac{\theta_{\mathrm{p}}\delta}{1-\delta} D_{\mathrm{p}}^2 F_{\mathrm{p}} - \frac{\pi^2\delta}{\sin(\pi\delta)} \theta_{\mathrm{p}}^{\delta} \lambda_{\mathrm{m}} (\mu_{\mathrm{m}}/\mu_{\mathrm{p}})^{\delta} D_{\mathrm{p}}^2}}{\pi\lambda_{\mathrm{p}} \frac{\theta_{\mathrm{p}}\delta}{1-\delta} F_{\mathrm{p}} + \frac{\pi^2\delta}{\sin(\pi\delta)} \theta_{\mathrm{p}}^{\delta} \lambda_{\mathrm{m}} (\mu_{\mathrm{m}}/\mu_{\mathrm{p}})^{\delta}}. \end{aligned} \tag{58}$$

where $F_{\mathrm{m}} = F(1, 1-\delta; 2-\delta; -\theta_{\mathrm{m}})$ and $F_{\mathrm{p}} = F(1, 1-\delta; 2-\delta; -\theta_{\mathrm{p}})$. When $\alpha = 4$, the above results can be simplified to

$$\epsilon_{\mathrm{m}} = 1 - \frac{1 - e^{-\pi\sqrt{\theta_{\mathrm{m}}} D_{\mathrm{m}}^2 \left(\lambda_{\mathrm{m}} \arctan\sqrt{\theta_{\mathrm{m}}} + \frac{\pi}{2}\lambda_{\mathrm{p}}\sqrt{\frac{\mu_{\mathrm{p}}}{\mu_{\mathrm{m}}}}\right)}}{\pi\sqrt{\theta_{\mathrm{m}}} D_{\mathrm{m}}^2 \left(\lambda_{\mathrm{m}} \arctan\sqrt{\theta_{\mathrm{m}}} + \frac{\pi}{2}\lambda_{\mathrm{p}}\sqrt{\frac{\mu_{\mathrm{p}}}{\mu_{\mathrm{m}}}}\right)}. \tag{59}$$

Then, for those PUs that actually have a serving PBS, the outage probability is

$$\epsilon_{\mathrm{p}}^{\mathrm{s}} = 1 - \frac{1 - e^{-\pi\sqrt{\theta_{\mathrm{p}}} D_{\mathrm{p}}^2 \left(\lambda_{\mathrm{p}} \arctan\sqrt{\theta_{\mathrm{p}}} + \frac{\pi}{2}\lambda_{\mathrm{m}}\sqrt{\frac{\mu_{\mathrm{m}}}{\mu_{\mathrm{p}}}}\right)}}{\pi\sqrt{\theta_{\mathrm{p}}} D_{\mathrm{p}}^2 \left(\lambda_{\mathrm{p}} \arctan\sqrt{\theta_{\mathrm{p}}} + \frac{\pi}{2}\lambda_{\mathrm{m}}\sqrt{\frac{\mu_{\mathrm{m}}}{\mu_{\mathrm{p}}}}\right)}. \tag{60}$$

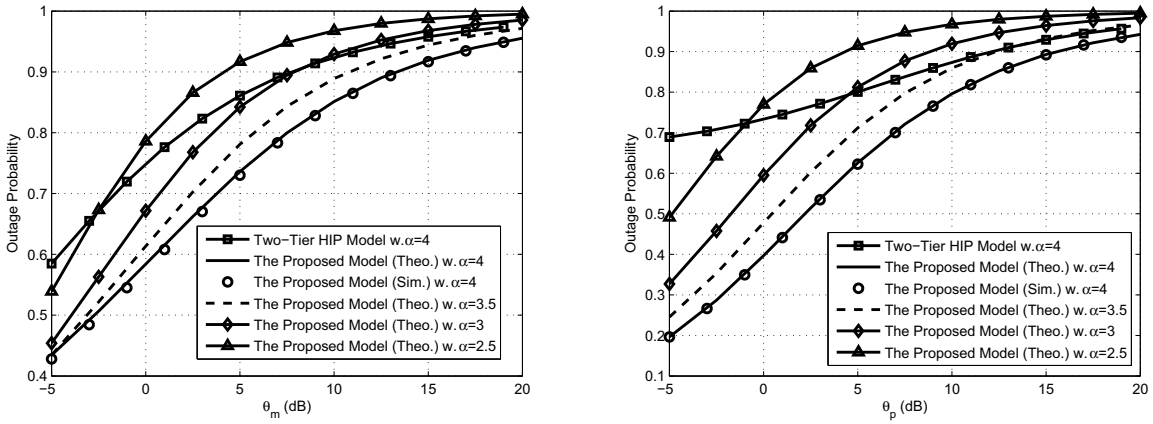

(a) Outage probability of MU.

(b) Outage probability of PU.

Fig. 15. Case 2: Model with intra-tier dependence for random serving distance.

Thus, the outage probability of an arbitrary PU can be obtained using Eq. (35).

For the per-user capacity, we have $c_{\rm m}=(1-\epsilon_{\rm m})\log_2(1+\theta_{\rm m})$ for the MU and $c_{\rm p}=(1-\epsilon_{\rm p})\log_2(1+\theta_{\rm p})$ for the PU, respectively. Thus, the per-user capacity for the two-tier HIP model is

$$c_{\rm u}=\frac{\lambda_{\rm m}(1-\epsilon_{\rm m})\log_2(1+\theta_{\rm m})+\lambda_{\rm p}(1-\epsilon_{\rm p})\log_2(1+\theta_{\rm p})}{\lambda_{\rm m}+\lambda_{\rm p}}. \tag{61}$$

Finally, the ASE for the two-tier HIP model is defined as

$$\text{ASE}=\lambda_{\rm m}(1-\epsilon_{\rm m})\log_2(1+\theta_{\rm m})+\frac{\lambda_{\rm p}N_{\rm p}}{\bar{c}(1+\lambda_l\pi R^2)}(1-\epsilon_{\rm p}^{\rm s})\log_2(1+\theta_{\rm p}). \tag{62}$$

In the following, we give some numerical results of the outage probability for MUs and PUs, the per-user capacity, and the area spectral efficiency for Case 2 with random serving distance, where $\lambda_{\rm m}=\lambda_l=8\times10^{-6}$, $\mu_{\rm m}=1$, $\mu_{\rm p}=0.05$, $\alpha=4$, $\bar{c}=20$, $R=(\pi(\lambda_{\rm m}+\lambda_l))^{-1/2}$. As a baseline, we also provide the performance of the two-tier HIP model with the same densities of the MBSs and the PBSs, and the same user distribution to show the effect of the intra-tier dependence on different performance metrics.

Figure 15 illustrates the outage probabilities of MUs and PUs for the intra-tier dependence model with random serving distance, respectively, where $\lambda_{\rm m}=\lambda_l=8\times10^{-6}$, $\mu_{\rm m}=1$, $\mu_{\rm p}=0.05$, $\bar{c}=20$, $R=(\pi(\lambda_{\rm m}+\lambda_l))^{-1/2}$. We can see that the simulation result matches the analytical result well, corroborating the accuracy of our theoretical analysis. As in the fixed-distance case, it can be observed that the model with larger α has lower outage due to the fast attenuations of the

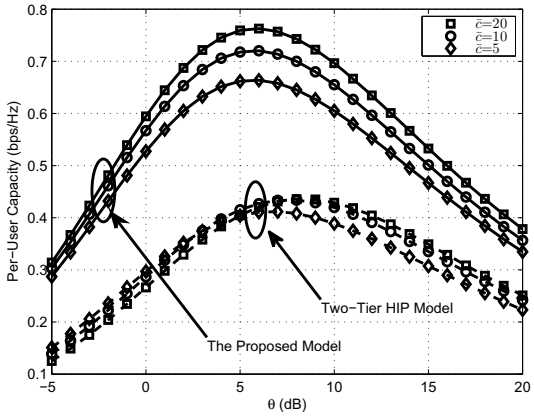

Fig. 16. Case 2: per-user capacity versus user threshold, where $\theta_{\mathrm{m}} = \theta_{\mathrm{p}} = \theta$.

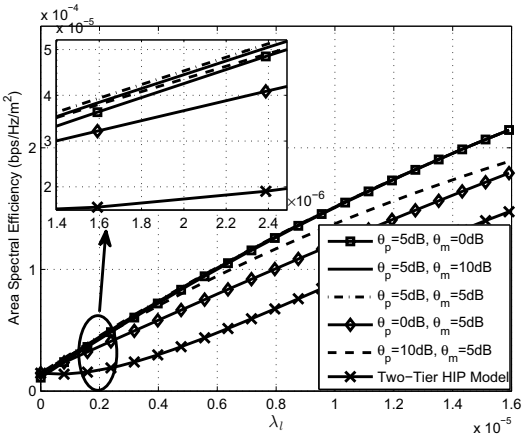

Fig. 17. Case 2: area spectral efficiency versus hotspot area fraction. For the two-tier HIP model, $\theta_{\mathrm{m}} = \theta_{\mathrm{p}} = 5\mathrm{dB}$.

interference signals. When $\alpha = 4$, for both the MU and PU, the outage performance of the proposed model with intra-tier dependence is superior than that of the two-tier HIP model.

Figure 16 shows the relationship between the per-user capacity and the user threshold ($\theta_{\mathrm{m}} = \theta_{\mathrm{p}} = \theta$) for different average numbers of PBSs per cluster $\bar{c}$. We can observe that for both models, i.e., the proposed model and the two-tier HIP model, the model with larger $\bar{c}$ has higher per-user capacity. This is because larger $\bar{c}$ means larger number of PBSs per cluster, reducing the distance between the PU and its serving PBS and thus increasing the desired signal strength, even though the interference from the PBSs may increase slightly at the same time. Therefore, both the MU and PU have smaller outage probability and further increase the per-user capacity. Furthermore, for each case of $\bar{c}$, the proposed model has higher per-user capacity than the two-tier HIP model since there are not enough PBSs for the many users in hotspot region when the PBSs are distributed as a PPP, which indicates that the model with intra-tier dependence is a more appropriate model than the two-tier HIP model for the HCNs where the traffic demand exhibits high spatial fluctuations.

Figure 17 depicts how the ASE changes with the hotspot area fraction for different thresholds of both MUs and PUs. We set $\lambda_{\mathrm{m}} + \lambda_l = 1.6 \times 10^{-5}$, then changing λ_l can be viewed as changing the ratio of the hotspot area to the whole network, i.e., the hotspot area fraction. It is seen that the ASE increases with λ_l. This is because, as λ_l increases, the hotspot area take more

proportion in the network and the capacity provided by the PBSs increases, leading to the rise of the ASE. When $\lambda_l = 1.6 \times 10^{-5}$, i.e., the HCN degrades into a single-tier network only with the PBSs deployed, all curves reach the peak, which indicates that putting a cluster of small cells at some location in the network may indeed deteriorate the outage due to the greater interference, but it will increase the ASE (which is related to the per-user capacity). From the comparison between the proposed model and the HIP model for $\theta_{\mathrm{m}} = \theta_{\mathrm{p}} = 5\mathrm{dB}$, we find that the two models have the same trend and basically maintain a fixed gap, which indicates that the HIP model underestimates the ASE of a HCN with hotspot regions and the Poisson cluster process is more appropriate for modeling the network where traffic demand has high spatial fluctuations. Besides, the effect of the PU threshold θ_{p} on the ASE becomes more noticeable as λ_l increases while the MU threshold θ_{m} is not, because the increase of λ_l leads to more PBSs and less MBSs deployed, hence leading the PBSs to be the main provider of the network capacity.

VI. Conclusion

In this paper, we proposed two HCN models with dependence: one is a two-tier HCN model with inter-tier dependence (Case 1), and the other is a two-tier HCN model with intra-tier dependence (Case 2). For Case 1, the MBS and the PBS deployments follow a PPP and a PHP (i.e., a Cox process), respectively, and the users are distributed in the whole plane according to another PPP. Due to the repulsion between the MBS tier and the PBS tier, the interference in the HCN is hard to analyze exactly. Thus, under this setup and conditioning on a fixed serving distance, we first bounded the outage probabilities of both MUs and PUs, and then used a fitted TCP to approximate the PHP. The results indicated that the bounds derived are very tight to the simulation curve and the approximations using the fitted TCPs coincide quite exactly with the simulation curve, thus providing useful approximations for a practical network model where an exact calculation of the interference is unfeasible. For Case 2, the MBSs and the PBSs follow a PPP and an independent MCP, respectively, while the users follow a Cox process where the user density in hotspots covered by PBSs is higher than in the rest of the network. Explicit expressions of the interference and the outage probability were derived with fixed serving distance, and the results indicated that the theoretical curves match the simulation results extremely well, corroborating the accuracy of the theoretical analysis.

To make the analysis more general and complete, we randomized the serving distance and

derived the outage performance, the per-user capacity, and the ASE for both cases. Results showed that the trends of the outage with random and fixed distances are the same, which means the more tractable analysis with fixed serving distance can be used to analyze and design the future HCNs sufficiently. Since the BS deployment is not changed, the PHP can still be approximated by the fitted TCP closely no matter whether the serving distance is fixed or not. More importantly, for case 1, the bounds and approximations with random serving distance are more tight and accurate to the simulation results than that with fixed serving distance. The comparisons between the model with intra-tier dependence (case 2) and the HIP model turn out that the HIP model underestimates the per-user capacity and the ASE by a factor of 1.5 to 2, which reveals that for a HCN with hotspot regions, ignoring the depends between the tiers (i.e., using the HIP model), leads to overly pessimistic results with significant errors. Notably, our work provides insight into the design and analysis of more practical HCN models, and the two models proposed provide good tradeoffs among the accuracy, tractability and practicability.

REFERENCES

[1] N. Deng, W. Zhou, and M. Haenggi, "A heterogeneous cellular network model with inter-tier dependence," in *IEEE Global Communications Conference (GLOBECOM'14)*, Texas, USA, Dec. 2014, accepted. Available at http://www.nd.edu/~mhaenggi/pubs/globecom14a.pdf.

[2] ——, "Outage and capacity of heterogeneous cellular networks with intra-tier dependence," in *International Conference on Wireless Communications and Signal Processing (WCSP'14)*, Hefei, China, Oct. 2014, submitted. Available at http://www.nd.edu/~mhaenggi/pubs/wcsp14.pdf.

[3] A. Ghosh *et al.*, "Heterogeneous cellular networks: From theory to practice," *IEEE Communications Magazine*, vol. 50, no. 6, pp. 54–64, 2012.

[4] M. Haenggi, *Stochastic geometry for wireless networks*. Cambridge University Press, 2012.

[5] H. ElSawy, E. Hossain, and M. Haenggi, "Stochastic geometry for modeling, analysis, and design of multi-tier and cognitive cellular wireless networks: A survey," *IEEE Communications Surveys & Tutorials*, vol. 15, no. 3, pp. 996–1019, 2013.

[6] J. G. Andrews, R. K. Ganti, M. Haenggi, N. Jindal, and S. Weber, "A primer on spatial modeling and analysis in wireless networks," *IEEE Communications Magazine*, vol. 48, no. 11, pp. 156–163, 2010.

[7] J. G. Andrews, F. Baccelli, and R. K. Ganti, "A tractable approach to coverage and rate in cellular networks," *IEEE Transactions on Communications*, vol. 59, no. 11, pp. 3122–3134, 2011.

[8] H. S. Dhillon, R. K. Ganti, F. Baccelli, and J. G. Andrews, "Modeling and analysis of K-tier downlink heterogeneous cellular networks," *IEEE Journal on Selected Areas in Communications*, vol. 30, no. 3, pp. 550–560, 2012.

[9] S. Mukherjee, "Distribution of downlink SINR in heterogeneous cellular networks," *IEEE Journal on Selected Areas in Communications*, vol. 30, no. 3, pp. 575–585, 2012.

[10] G. Nigam, P. Minero, and M. Haenggi, "Coordinated Multipoint Joint Transmission in Heterogeneous Networks," *IEEE Transactions on Communications*, 2014, submitted. Available at http://www.nd.edu/~mhaenggi/pubs/tcom14.pdf.

[11] M. Haenggi, "The mean interference-to-signal ratio and its key role in cellular and amorphous networks," Jun. 2014, submitted. Available at http://arxiv.org/pdf/1406.2794.pdf.

[12] I. Nakata and N. Miyoshi, "Spatial stochastic models for analysis of heterogeneous cellular networks with repulsively deployed base stations," *Performance Evaluation*, 2014.

[13] N. Deng, W. Zhou, and M. Haenggi, "The Ginibre point process as a model for wireless networks with repulsion," *IEEE Transactions on Wireless Communications*, 2014, accepted. Available at http://www.nd.edu/~mhaenggi/pubs/twc14c.pdf.

[14] C.-H. Lee and M. Haenggi, "Interference and outage in Poisson cognitive networks," *IEEE Transactions on Wireless Communications*, vol. 11, no. 4, pp. 1392–1401, 2012.

[15] 3GPP:R1-100701, "Importance of serving cell association in HetNets," *Qualcomm Inc.*, Jan. 2010.

[16] N. Deng, S. Zhang, W. Zhou, and J. Zhu, "A stochastic geometry approach to energy efficiency in relay-assisted cellular networks," in *IEEE Global Communications Conference (GLOBECOM'12)*, 2012, pp. 3484–3489.

[17] Y. Zhong and W. Zhang, "Multi-channel hybrid access femtocells: A stochastic geometric analysis," *IEEE Transactions on Communications*, vol. 61, no. 7, pp. 3016–3026, July 2013.

[18] A. Jeffrey and D. Zwillinger, *Table of integrals, series, and products*. Academic Press, 2007.

[19] M. Haenggi, "Mean interference in hard-core wireless networks," *IEEE Communications Letters*, vol. 15, no. 8, pp. 792–794, 2011.

[20] R. Ganti and M. Haenggi, "Interference and outage in clustered wireless ad hoc networks," *IEEE Transactions on Information Theory*, vol. 55, no. 9, pp. 4067–4086, 2009.

[21] A. Papoulis and S. U. Pillai, *Probability, random variables, and stochastic processes*. Tata McGraw-Hill Education, 2002.

[22] M. Haenggi, J. G. Andrews, F. Baccelli, O. Dousse, and M. Franceschetti, "Stochastic geometry and random graphs for the analysis and design of wireless networks," *IEEE Journal on Selected Areas in Communications*, vol. 27, no. 7, pp. 1029–1046, 2009.